Received: 2 March 2022 | Revised: 27 June 2022 | Accepted: 24 July 2022

DOI: 10.1111/bre.12702

Basin Research | EAGE | WILEY

RESEARCH ARTICLE

A song of volumes, surfaces and fluxes: The case study of the Central Mallorca Depression (Balearic Promontory) during the Messinian Salinity Crisis

Fadl Raad[1] | **Ronja Ebner**[2] | **Hanneke Heida**[3,4] | **Paul Meijer**[2] | **Johanna Lofi**[1] | **Agnès Maillard**[5] | **Daniel Garcia-Castellanos**[3]

[1]Géosciences Montpellier, Université de Montpellier, CNRS, Montpellier Cedex 05, France

[2]Department of Earth Sciences, Utrecht University, Utrecht, The Netherlands

[3]Geosciences Barcelona (GEO3BCN-CSIC), Barcelona, Spain

[4]Departament de Dinàmica de la Terra i de l'Oceà, Universitat de Barcelona, Barcelona, Spain

[5]Géosciences Environnement Toulouse GET, OMP, Université de Toulouse, CNRS, IRD, Toulouse, France

Correspondence
Ronja Ebner, Department of Earth Sciences, Utrecht University, Princetonlaan 8A 3584 CB Utrecht, The Netherlands.
Email: r.m.ebner@uu.nl

Funding information
EXCELLENT SCIENCE - Marie Skłodowska-Curie Actions, Grant/Award Number: 765256

Abstract

The Central Mallorca Depression (CMD) located in the Balearic Promontory (Western Mediterranean) contains a well-preserved evaporitic sequence belonging to the Messinian Salinity Crisis (MSC) salt giant, densely covered by high- and low-resolution seismic reflection data. It has been proposed recently that the MSC evaporitic sequence in the CMD could be a non-deformed analogue of the key MSC area represented by the Caltanissetta Basin in Sicily. This presumed similarity makes the CMD an interesting system to better understand the MSC events. Physics-based box models of the water mixing between sub-basins, built on conservation of mass of water and salt, help constrain the hydrological conditions under which evaporites formed during the MSC. Those models have been widely used in the literature of the MSC in the past two decades. They have been mostly applied to the Mediterranean Sea as a whole focusing on the Mediterranean–Atlantic connection, or focusing on the influence of the Sicily Sill connecting the Western and Eastern Mediterranean Sea. In this study, we apply a downscaled version of such modelling technique to the CMD. First, we quantify the present-day volumes of the MSC units. We then use a reconstructed pre-MSC paleo-bathymetry to model salinity changes as a function of flux exchanges between the CMD and the Mediterranean. We show that a persistent connection between the CMD and the Mediterranean brine near gypsum saturation can explain volume of Primary Lower Gypsum under a sea level similar to the present. For the halite, on the contrary, we show that the observed halite volume cannot be deposited from a connected CMD-Mediterranean scenario, suggesting a drawdown of at least 850 m (sill depth) is necessary. Comparison between the deep basin halite volume and that of the CMD shows that it is possible to obtain the observed halite volume in both basins from a disconnected Mediterranean basin

Fadl Raad and Ronja Ebner contributed equally as first authors.

undergoing drawdown, although determining the average salinity of the Western Mediterranean basin at the onset of drawdown requires further investigation.

KEYWORDS

Central Mallorca Depression, evaporites, Messinian Salinity Crisis, modelling

1 | INTRODUCTION

The reduction of water exchange between the Atlantic and Mediterranean caused by the tectonic uplift of the Gibraltar arc during the Late Miocene Messinian Salinity Crisis (MSC; 5.97–5.33 Ma) led to the deposition of a large evaporitic body, also known as the Mediterranean Salt Giant, in a relatively short geological time interval of ca. 640 kyr (CIESM, 2008; Hsü, 1973; Krijgsman et al., 1999; Ryan, 1973). It has been suggested that deposition of the Mediterranean MSC salt giant has greatly affected the global oceans, by sequestering up to ca. 6%–10% of their salt content into the Mediterranean Sea (Garcia-Castellanos & Villaseñor, 2011; Haq et al., 2020). The mechanisms and time spans for the deposition of the MSC evaporites are still not clear and highly debated despite the numerous studies in the last half century, although a generally accepted chronostratigraphic model that divides the MSC events into three stages has been proposed (CIESM, 2008; Roveri, Flecker, et al., 2014). According to this model, the onset of the MSC is marked, at least in marginal basins (<200 m paleo-depth), by up to 16 precessionally driven cycles of gypsum intercalated with marls/carbonates, also called the Primary Lower Gypsum (PLG). The deposition of the PLG took place during the first stage of the MSC (stage 1; 5.971–5.60 Ma; Krijgsman et al., 1999; Lugli et al., 2010). It was followed by stage 2 (5.60–5.55 Ma), in which part of the PLG was removed (by erosion and/or as mass transport deposit) and resedimented as Resedimented Lower Gypsum (RLG) (Clauzon et al., 2015; Manzi, Roveri, et al., 2021; Roveri et al., 2006), and a halite unit was deposited in intermediate (ca. 200 to 1000 m paleo-depth; e.g., Caltanissetta Basin and Central Mallorca Depression; Lugli et al., 1999; Raad et al., 2021) to deep basins (>1000 m paleo-depth; e.g., Provencal and Levant basins; Lofi et al., 2011). During this stage, margins and slopes underwent intense erosion of subaerial origin according to some authors (e.g., Clauzon, 1978; Lofi et al., 2005) or of submarine origin according to others (e.g., Roveri, Manzi, et al., 2014). The third and last MSC stage is divided in two substages, substage 3.1 (5.55–5.42 Ma) in which the Upper Evaporites (UE) deposited in hypersaline conditions (Manzi et al., 2009), and substage 3.2 (5.42–5.33 Ma) which witnessed more hyposaline conditions, also known as the Lago Mare phase (Andreetto et al., 2021).

Highlights

- Gypsum saturation was reached in the upper layer of the Mediterranean during stage 1 of the Messinian Salinity Crisis.
- Primary Lower Gypsum deposition was not limited to shallow (<200 m) silled basin.
- A high amplitude drawdown >850 m occurred in the Western Mediterranean during the second stage of the crisis.
- Halite emplacement in the intermediate basins is diachronous from the deep basin halite.

Several aspects and implications of the consensus model remain ambiguous and continuously questioned. For example, whether the halite deposition took place synchronously and exclusively during stage 2 (Manzi et al., 2018; Manzi, Gennari, et al., 2021; Roveri, Flecker, et al., 2014) or started already during stage 1 (Meilijson et al., 2018, 2022). Another controversy is whether the isolated conditions persisted during the whole stage 3 or the Atlantic–Mediterranean connection was restored at the beginning of that stage (Andreetto et al., 2021), with a Mediterranean probably supplied also by Paratethyan brackish water (Marzocchi et al., 2016). Many more aspects continue to puzzle regarding the MSC: the amplitude and duration of the main water level drawdown, the reason for the absence of evaporites on most of the shelves and slopes of the open deep basins, the cause of lack of a clear paleo-depth distribution of halite (e.g., deep halite-free Valencia Basin versus shallower Balearic Promontory containing halite; Heida et al., 2021).

The Balearic Promontory (BP), a prominent high in the Western Mediterranean (Figure 1), presents a unique opportunity to investigate the formation of the MSC evaporites, thanks to the well-preserved evaporitic units deposited since the beginning of the crisis (Driussi, Maillard, et al., 2015; Maillard et al., 2014; Ochoa et al., 2015; Raad et al., 2021). Lying between Mallorca and Ibiza, the Central Mallorca Depression (CMD) contains the most complete and least tectonically deformed evaporitic sequence in the

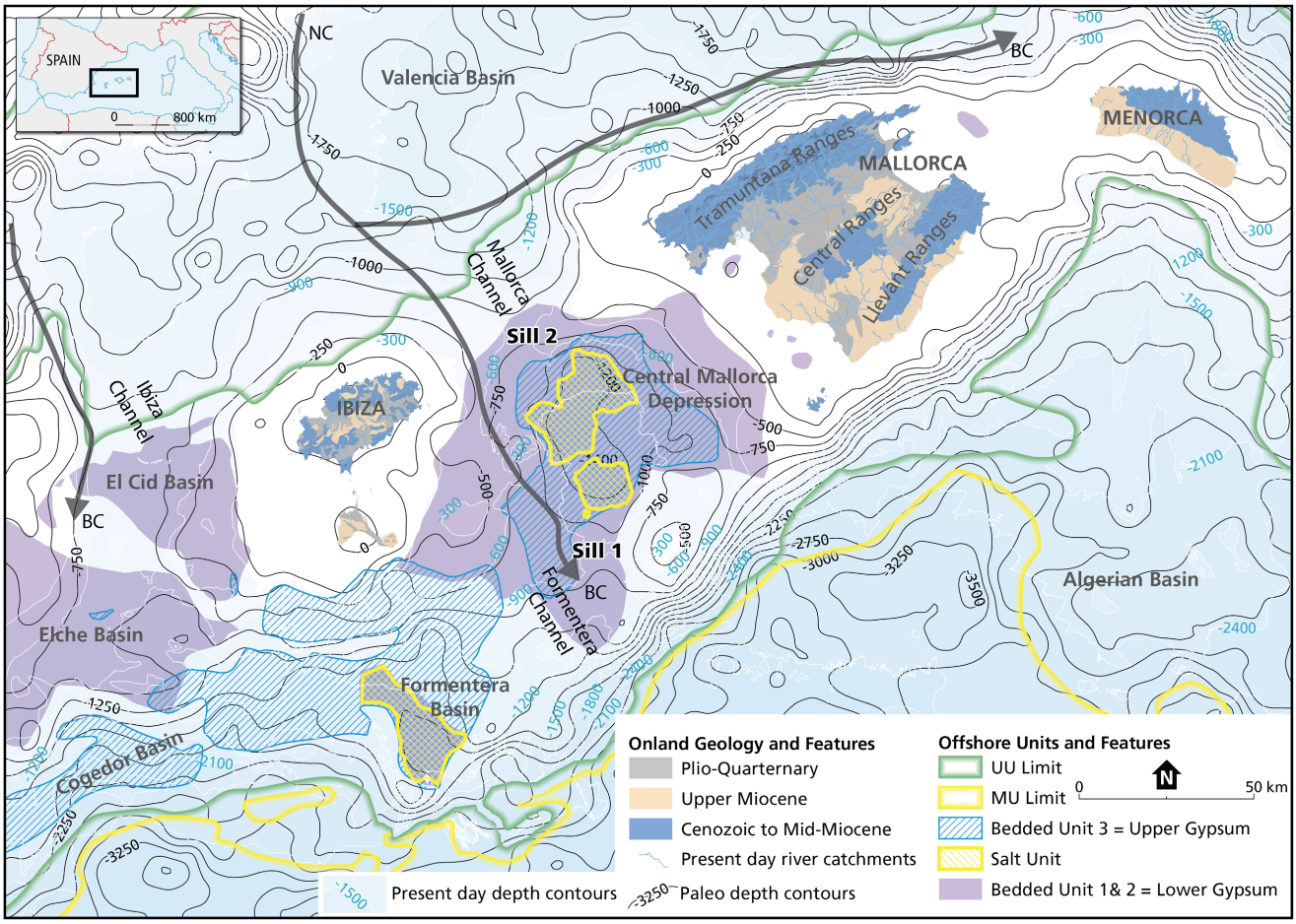

FIGURE 1 Map of the MSC units over the Balearic Promontory (BP), Valencia Basin and Algerian Basin. Our study area focuses on the Central Mallorca Depression (CMD) located between the islands of Mallorca and Ibiza, which contains several Bedded Units (BUs) and a Halite unit geometrically/attitudinally separated from the deep basin's Mobile Unit (MU) and Upper Unit (UU). MSC units of the BP are modified from Raad et al. (2021). Onland geology of the Balearic Islands is modified from geological map of Spain 1:50000 (IGME). Thin white lines in the background represent the present-day Bathymetry taken from the European Marine Observation and Data network (EMODnet) database available online (www.emodnet-bathymetry.eu). Thin black lines represent the paleo-bathymetry at the start of the MSC, modified after Heida et al. (2021). Arrows indicate the present day currents (from Pinot et al. (2002) and Lüdmann et al. (2012)). BC, Balearic Current; NC, Northern Current.

BP, including halite (Maillard et al., 2022; Raad et al., 2021). This sequence has been studied and accurately mapped recently by several authors (Figure 1) (Driussi, Maillard, et al., 2015; Maillard et al., 2014; Raad et al., 2021). Most recently, Raad et al. (2021) showed that the MSC evaporitic sequence in the CMD could be an undeformed analogue of the intermediate-depth Caltanissetta Basin in Sicily, a rare example of onshore record holding MSC halite, which makes the CMD an interesting place to study for furthering our understanding of the MSC.

Physics-based models help in examining some hydrological factors under which the MSC evaporites formed. Those models have been widely used in MSC research in the past two decades (Blanc, 2000, 2006; Krijgsman & Meijer, 2008; Meijer, 2006, 2012; Meijer & Krijgsman, 2005; Simon et al., 2017; Topper et al., 2011; Topper & Meijer, 2013). All those studies worked on a Mediterranean scale aimed at the Atlantic-Western Mediterranean and Western-Eastern Mediterranean connections through the Gibraltar and Sicily straits, respectively. In this study, we scale down as we apply models based on conservation of mass of water and salt and a simplified representation of strait dynamics, on a single sub-basin within the Western Mediterranean, the CMD (Figure 1). A similar approach has been applied recently in the Sorbas Basin using such models by Modestou et al. (2017). In the CMD, the presence of a good, high- and low-resolution seismic reflection data coverage allows the determination of the thicknesses and respective volumes of the evaporites (Figure 2a). In addition, the availability of a restored pre-MSC paleobathymetry published recently by Heida et al. (2021), allows the establishment of the hypsometry of the basin during the MSC.

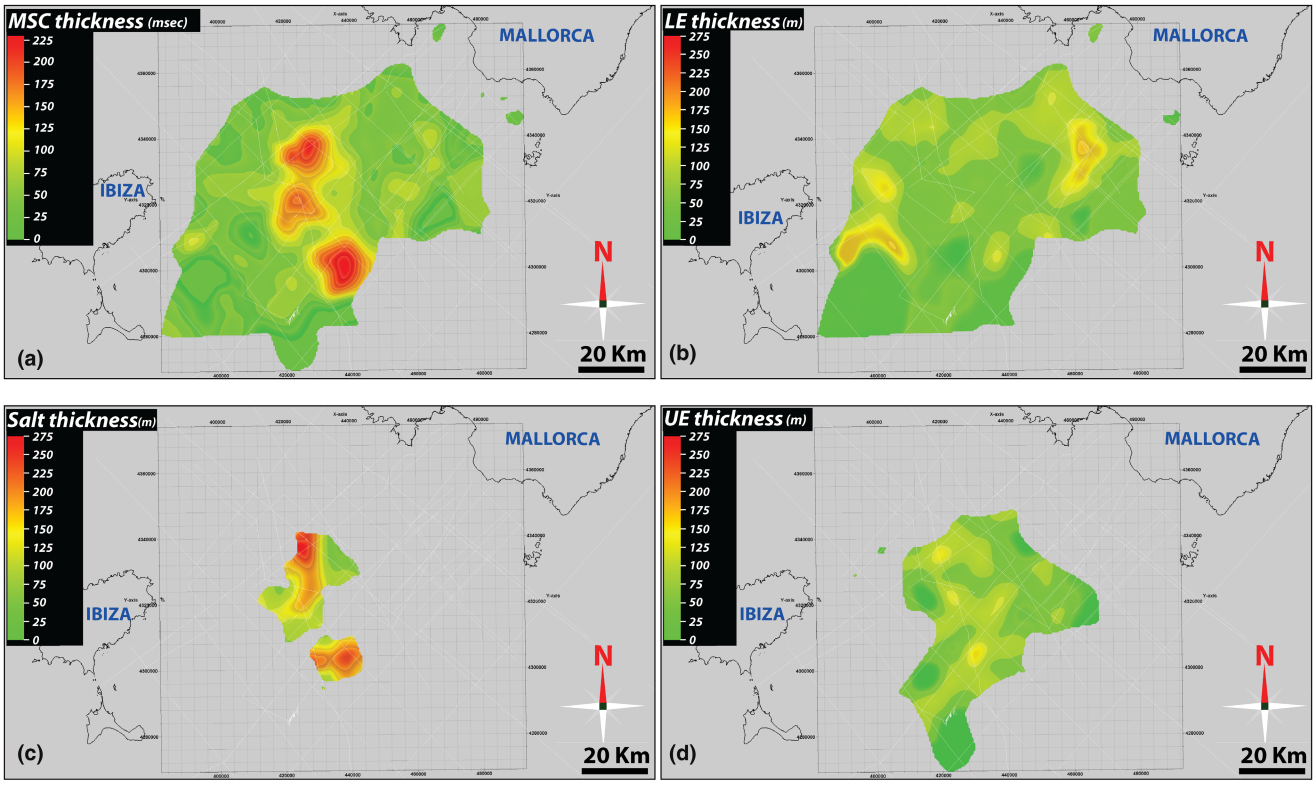

FIGURE 2 Thickness maps of the MSC units of the CMD. (a) Thickness map in TWTT of the whole MSC units, including all BUs and Halite in TWTT. (b) Thickness map in metres of BU1 + BU2 interpreted as stage 1 MSC Lower Evaporites (LE), with gypsum content ranging between of about 80% (see text and Table 1 for explanation). (c) Thickness map in metres of the halite unit. (d) Thickness map in metres of BU3 interpreted as MSC stage 3 Upper Evaporites (UE). The white thin lines mark the locations of seismic profiles used to map the deposits.

The main objectives of this study are to: (1) establish the hydrological conditions (salinity and fluxes) and mechanisms under which the evaporites (gypsum and halite) in the CMD formed during MSC stages 1 and 2, and (2) examine the amplitude of a potential water level drawdown in the CMD needed to explain the required hydrological conditions.

To reach these objectives, we use the calculated volumes of the MSC evaporites and the restored pre-MSC bathymetry to (1) make water budget calculations of the CMD and compare those with the observed evaporitic volumes, (2) test the factors (fresh water budget and fluxes) controlling the salinity of the CMD as an isolated basin, (3) calculate the fastest evolution possible of the CMD and Valencia Basin in terms of salinity and time to deposit the observed evaporites, and (4) discuss our results and observations in the frame of the whole Mediterranean Salt Giant complex and compare them to the consensus model.

2 | GEOLOGICAL BACKGROUND

The present-day BP is characterized by a series of sub-basins lying at a wide range of depths (Figure 1; e.g., −650 m Elche Basin and −1700 m Formentera Basin). They show different levels of inter-basinal connection and all contain MSC sediments up to ca. 500 m thick (Figures 1 and 2; Driussi, Briais, & Maillard, 2015; Ochoa et al., 2015; Raad et al., 2021). The MSC sediments of the BP have been mainly studied through seismic reflection data due to the absence of exploratory scientific boreholes. They consist of Bedded Units covering most of the BP area (BU sensu Lofi, 2018; Lofi et al., 2011; divided subsequently into BU1, BU2 and BU3 by Raad et al., 2021; Table 1) as well as salt patches present in some sub-basins depocentres (Figure 1) (Acosta et al., 2004; Driussi, Maillard, et al., 2015; Heida et al., 2021; Maillard et al., 2014; Mauffret, 1977; Raad et al., 2021). The sub-basins are believed to have inherited their structure from the pre-Messinian tectonic evolution of the promontory, and thus to have been preexisting topographic lows during the MSC allowing the accumulation of evaporites (Driussi, Briais, & Maillard, 2015; Sàbat et al., 2011).

In this work, we focus mainly on the CMD, an intermediate-depth (sensu Roveri, Flecker, et al., 2014) sub-basin containing a well-preserved MSC sequence.

TABLE 1 Characteristics and parameters of the MSC units present in the CMD

MSC unit	Interpreted lithology	MSC stage and duration	Velocity for TWTT to depth conversion	Evaporites/clastic ratio	Total volume (m^3)	Evaporitic volume (m^3)	Thickness (metres)	Bounding surfaces
BU1 = LE (PLG)	Selenitic gypsum intercalated with marls	Stage 1 (5.97–5.60 Ma)	4500 m/s (Ochoa et al., 2015)	80%	3.73E+11	2.99E+11	40–180 m	Base: Conformable Top: TES
BU2 = LE	Pelagic gypsum intercalated with marls	Stage 1 (5.97–5.60 Ma)	4500 m/s	80%	3.73E+11	2.99E+11	40–180 m	Base: Conformable Top: Conformable
Salt unit	Halite	Stage 2 (5.60–5.55 Ma)	4780 m/s (Samperi et al., 2020)	100%	9.63E+10	9.63E+10	280 m	Base: Conformable Top: IES
BU3 = UE + LM?	Alternations of gypsum and clastics	Stage 3 (5.55–5.33 Ma)	3500 m/s	50%	1.63E+11	8.14E+10	150 m	Base: IES Top: Conformable

Abbreviations: BU, bedded unit; IES, intermediate erosion surface; LE, lower evaporites; LM, Lago Mare; PLG, primary lower gypsum; TES, top erosion surface; UE, upper evaporites.

2.1 | The Central Mallorca Depression: Present-day versus paleo-topography

Today, the maximum water depth of the CMD reaches −1050 m (Figure 1; Acosta et al., 2004). The CMD is surrounded by the gently dipping slopes of Mallorca and Ibiza to the NNE and WSW, respectively. It is connected northward to Valencia Basin through the ca. 730 m deep, ca. 20 km wide Mallorca Channel (Pinot et al., 2002), and southward to the Algerian Basin through the ca. 1000 m deep, ca. 30 km wide channel that we call the Formentera Channel (Figure 1). The CMD underwent limited post-MSC tectonics with some local deformation caused by extension and strike-slip motions (Acosta et al., 2004; Sàbat et al., 2011), which guaranteed a good preservation of the MSC deposits. Other sources of vertical motions, such as isostatic subsidence, compaction and thermal subsidence, did not strongly affect the CMD due to the nature of the lithosphere below the BP and the limited extent and thickness of the sediments (Heida et al., 2021 and references therein). Heida et al. (2021) applied a pseudo-3D backstripping restoration of the Messinian paleo-topography of a large area in the Western Mediterranean, including the BP. They obtained pre-MSC paleo-depths of the BP sub-basins ranging from ca. 550 m (e.g., Cogedor Basin) to ca. 1800 m (e.g., Formentera Basin). The CMD was at ca. 1500 m in its deepest part (Figures 1, 3 and Table 3; Heida et al., 2021), whereas the Mallorca and Formentera channels were at 750 m and 850 m (±50 m; Heida et al., 2021) respectively (Sill 02 and Sill 01, respectively, in Figures 1 and 3).

2.2 | Present-day hydrography and water masses in the Central Mallorca Depression

Generally, four water masses can be distinguished in the Western Mediterranean: the Modified Atlantic Surface Water; the Levantine Intermediate Water; the Western Mediterranean Deep Water; and the Bottom Water (La Violette, 1994; Lüdmann et al., 2012; Pinot et al., 2002). The Mallorca and Ibiza channels play a main role in the regional water exchange and circulation of those water masses. In particular, the Northern Current carrying northern waters from the Gulf of Lions southward along the continental slope of the Valencia Basin is in part blocked by the Balearic Islands and consequently bifurcates north of Ibiza. One branch, called the Balearic Current, passes through the Ibiza and Mallorca channels into the Algerian Basin (Figure 1). Several studies surveyed and quantified the present-day oceanographic parameters of these currents (water exchanges, fluxes, salinities) across the Mallorca Channel (Barceló-Llull et al., 2019; Pinot et al., 2002; Vargas-Yáñez et al., 2020).

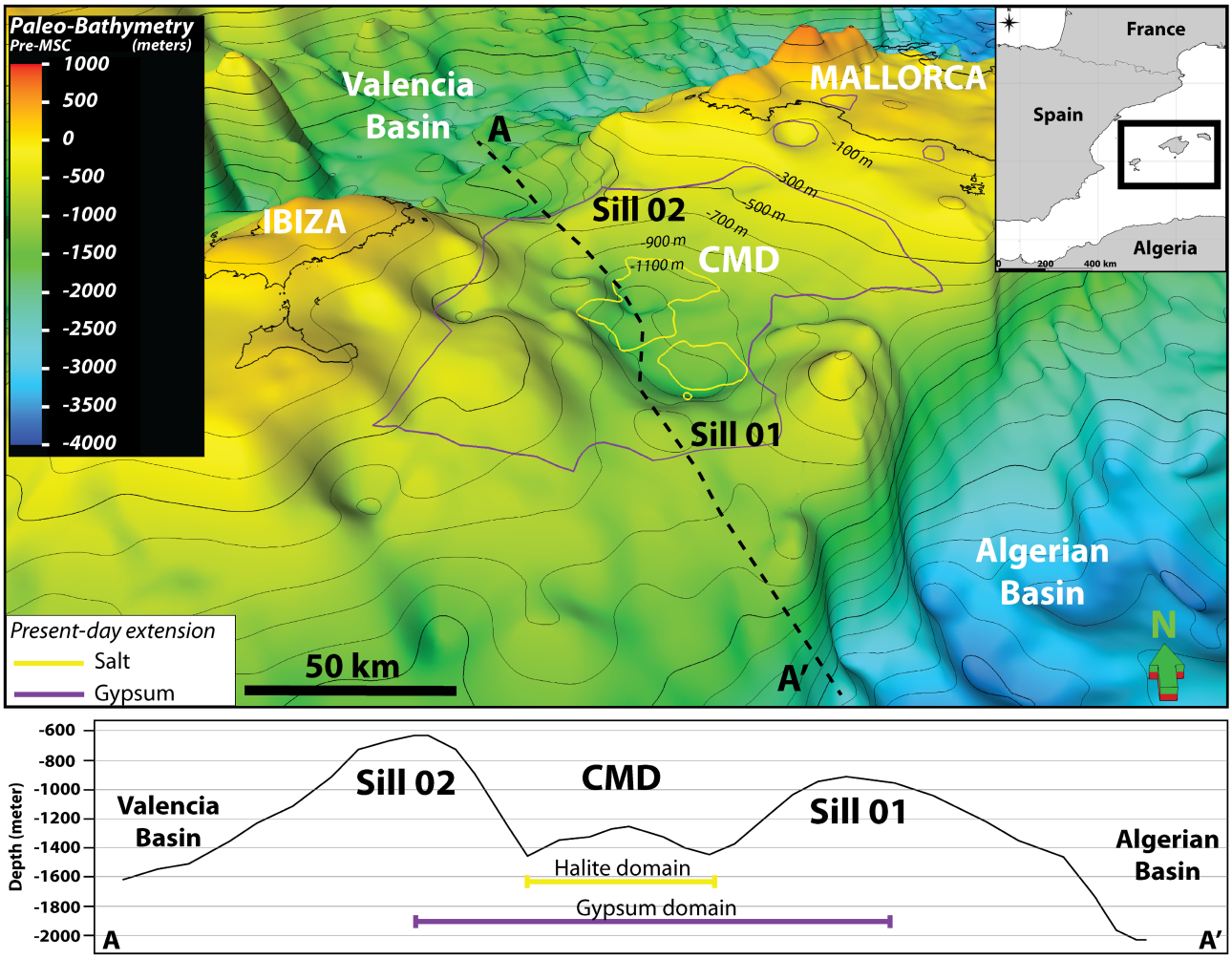

FIGURE 3 3D paleo-bathymetry of the CMD at the beginning of the MSC. The CMD is connected to the deep basin through two silled channels/connections. Sill 01 is deeper and is the one that is used in the modelling as a connection between the CMD and the open Mediterranean. A-A′ is a 2D profile highlighting the geometry of the CMD and the sills. The violet and yellow polygons represent the present-day extension of the gypsum and halite, respectively. They are 2D polygons projected above the 3D paleo-bathymetry.

The fresh water from river runoff reaching the CMD is very limited (<<10 m^3/s; Table 3) with minor river catchments draining from the Tramuntana and Central ranges onshore Mallorca, and the central part of Ibiza Island (Figure 1; Garcia et al., 2017 and references therein). Most of the catchments are draining mainly Mesozoic carbonates (Figure 1).

2.3 | Messinian Salinity Crisis in the Central Mallorca Depression

So far, only two studies were dedicated to the MSC deposits in the CMD. Maillard et al. (2014) were the first to study and map the BUs and to image the salt offshore at an intermediate depth. The authors present all possible scenarios for the deposition of the MSC sediments based on the observed features and markers (see their Figure 12). In the most recent study dedicated to the MSC deposits in the BP, Raad et al. (2021) made a step forward by dividing the BUs into three sub-units (Table 1) based on their seismic-stratigraphic position and seismic facies. Including the salt unit, they performed a unit-by-unit comparison to the MSC evaporites outcropping in the Sicilian Caltanissetta Basin. Following their division and comparison, Raad et al. (2021) interpreted the MSC units of the CMD and proposed a depositional model as follows (see their Figure 10 and discussion for a detailed description and interpretation of each unit):

- BU1: equivalent to the PLG and deposited during stage 1 of the MSC (Table 1). It is the only drilled MSC unit of the BP and is made of a succession of precession-driven cycles of selenitic gypsum and marls (Ochoa et al., 2015). This unit is topped by a clear erosional surface everywhere on the BP (Maillard et al., 2014; Ochoa et al., 2015; Raad et al., 2021). In the CMD, BU1 reaches a maximum thickness of ca. 180 m in

the proximal domain (Figure 2b) when it is preserved. It thins towards the distal domain (ca. 40 m), and/or where it is eroded by paleo-incisions (Figure 2b; Raad et al., 2021).

- BU2: possible time equivalent of BU1 (i.e., MSC stage 1), it would represent its distal facies equivalent. According to Raad et al. (2021), this unit likely consists mainly of cumulate gypsum, alternated with non-evaporitic sediments. The cumulate gypsum is commonly known to form in a supersaturated water column in which gypsum crystals nucleate at the top or within water column and then precipitate and settle on the seafloor as laminar gypsum (Bąbel & Schreiber, 2014; Hardie & Lowenstein, 2004; Natalicchio et al., 2021). No erosional features mark the top or the base of this unit. Both BU1 and BU2 were deposited during a high stand and then followed by an important base level drawdown, during which only BU1 was exposed.
- Salt unit: it consists mainly of halite and might include more soluble salts (K- and Mg- salts), similar to the salts observed in Caltanissetta Basin (Lugli et al., 1999; Manzi et al., 2012). The salt unit in the CMD is truncated at its upper limit by an erosional surface, probably due to exposure and/or dissolution in relatively shallow water when the maximum base level drawdown was reached. It reaches a maximum thickness of ca. 280 m in the deepest depocentre (Figure 2c).
- BU3: this unit is interpreted as the equivalent of the Upper Evaporites of the Caltanissetta Basin, and consisting of alternating terrigenous and gypsum beds deposited during stage 3 of the MSC (Table 1). It lies unconformably above the BU1 and the salt. It lies conformably below the lowermost Pliocene pelagic sediments. BU3 reaches thicknesses up to ca. 170 m (Figure 2d). It shows no physical relationship or continuation with the deep basin's MSC evaporites. For this reason Raad et al. (2021) and Heida et al. (2021) concluded that the CMD was disconnected from all the surrounding basins during the final stage of the MSC, before getting reconnected during the Zanclean reflooding with the rest of the Mediterranean at the end of the crisis (Garcia-Castellanos et al., 2009). In this scenario, the sulphate ions needed for gypsum precipitation are exclusively derived from dissolution of stage 1 PLG (Andreetto et al., 2021; Ryan, 2009).

3 | DATA AND METHODS

3.1 | Seismic dataset and volume calculations

We use widespread high- and low-resolution seismic reflection profiles to calculate the volumes of the MSC units in the CMD (Figure 2a). This dataset has been interpreted, described and used in several previous studies (e.g., Bellucci et al., 2021; Maillard et al., 2014; Raad et al., 2021). Following the interpretation of the MSC units on the seismic profiles, a thickness map for each unit was created (Figure 2) using the internal velocities presented in Table 1 for the time to depth conversion.

For the volume calculations, we consider 80% of the total volume of BU1 (=PLG) and BU2 as gypsum, since elsewhere around the Mediterranean the PLG cycles contain only thin non-evaporitic intercalations and much thicker gypsum beds (Table 1; e.g., Lugli et al., 2010; Ochoa et al., 2015 for the BP offshore area; García-Veigas et al., 2018; Mas & Fornós, 2020). For the BU3 (=UE) we consider only 50% of its volume as gypsum since the gypsum:non-evaporitic deposit ratio of the UE is lower than the PLG (Table 1; e.g., Manzi et al., 2009 for Sicily; Manzi et al., 2016 for Cyprus; Lugli et al., 2015 for the Upper Unit in offshore DSDP and ODP sites). No such assumptions are made for the halite volume as we consider the entire salt unit as made of halite with negligible amount of clastics (Lugli et al., 1999; Manzi et al., 2012; Samperi et al., 2020).

3.2 | Theoretical model

Investigating the possible scenarios that could have led to the Messinian deposits of the CMD requires that we consider the salinity of the basin itself as well as the salinity of the surrounding waters. In this study, we define salinity (S) as dissolved mass of salts (m) per volume of water (V), ($S = m/V\,[\mathrm{kg/m^3}]$).

We treat salinity as a sum of concentrations and differentiate between the salts of interest, i.e., gypsum and halite:

$$S = \frac{\sum m_{\mathrm{Salts}}}{V} = \sum [\mathrm{salt}] = c\left[\mathrm{CaSO_4}\right] + c[\mathrm{NaCl}] + c[\mathrm{other\ salts}] \quad (1)$$

Since the exact composition of seawater during the MSC is not known, we use a composition that has been used in previous studies (e.g., Gladstone et al., 2007; Krijgsman & Meijer, 2008; Simon et al., 2017; Topper & Meijer, 2013) and assume a proportional increase of the partial concentrations with increasing salinity, until saturation is reached. Saturation is defined as the salinity at which the water body cannot hold any extra ions of the salt in question. Adding the concentration of the three ion groups (Table 2) to Equation (1), we define our reference salinity to be $S_{\mathrm{reference}} = 35.05\ \mathrm{kg/m^3} = 1.27\ \mathrm{kg/m^3} + 27.21\ \mathrm{kg/m^3} + 6.57\ \mathrm{kg/m^3}$ (Leeder, 2009). Assuming seawater is saturated in gypsum at 145 $\mathrm{kg/m^3}$ (De Lange et al., 1990;

McCaffrey et al., 1987) and in halite at 350 kg/m^3 (Bąbel & Schreiber, 2014; McCaffrey et al., 1987), we can then calculate the saturation concentration for gypsum, $c\left[CaSO_4\right]^{sat} = 5.25\ kg/m^3$ and halite $c[NaCl]^{sat} = 272.1\ kg/m^3$ (Krijgsman & Meijer, 2008; Topper & Meijer, 2013). A direct application of these values is to quantify the volume of water, at saturation concentration, that would be needed to form an observed volume of deposit. Since a lower concentration would require a bigger volume of water to precipitate the deposit, this water volume at saturation will be called V_{min}:

$$V_{min} = \frac{m_{salt}}{c[salt]^{sat}} = \frac{V_{deposit} * \rho_{deposit}}{c[salt]^{sat}} \quad (2)$$

In which m_{salt} is the salt mass that forms the deposit that can be derived from the volume of the deposit, $V_{deposit}$ in [m^3] and its density, $\rho_{deposit}$ [kg/m^3] (Table 2).

The water volume of the CMD is defined by the physical limits of the basin as retrieved from the pre-Messinian paleo-bathymetry of the CMD (Figure 3) (Heida et al., 2021). From the same reconstruction, we draw cross sections through the southern and the northern connection between the CMD and the adjacent Mediterranean Sea. With a width of 70–80 km at sea level and a depth of up to 850 m, these connections are larger than the Strait of Gibraltar (12 km wide, 300 m deep; Lacombe & Richez, 1982). They are best described as wide openings with a sill that is elevated well above the seafloor north and south of the CMD but still located at significant water depth (Figure 3). The openings would form a narrow strait and/or shallow sill only when the water level is significantly lower than today. From modern measurements (Barceló-Llull et al., 2019; Pinot et al., 2002), it is known that there are both fluxes into and out of the basin through each of the two connections (see Section 2.2).

It is possible to apply basic principles that allow us to learn about the CMD and its fluxes as a system while making as little assumptions as possible. One of these principles is the conservation of water volume for a system that is in balance. This means that the volume of water in the basin does not change when the sum of fluxes into the basin is of the same size as the sum of outward fluxes. In contrast, when there is a net outflux, the volume of water inside the basin will decrease over time, with a rate defined by the absolute difference between the in- and outflux. This is for example the case for a disconnected basin with a negative freshwater budget. This loss of fresh water is described by a volume flux [m^3/s] (positive when the basin loses water) and named freshwater budget (fwb).

$$fwb = (E - P) * A - R \quad (3)$$

In which E is the rate of evaporation [m/s], P the rate of precipitation [m/s], A the surface area of the basin [m^2] and R the inflow of river water [m^3/s]. In this scenario, the basin experiences a drawdown due to the loss of water volume to the atmosphere (Figure 4a) until the surface area A is so small that the net evaporative loss is of the same size as the river inflow R. When the water volume decreases, the salinity increases until an equilibrium is reached, since neither net evaporation nor river inflow transport ions. In this case, the evolution of salinity S with time t is given by,

TABLE 2 Parameters used in our modelling for Halite and Gypsum with the corresponding references

	Gypsum	Halite	References
Density (kg/m^3)	2300	2200	Leeder (1999)
Fraction of Iongroup (−)	1.27/35	27.21/35	Leeder (1999), Topper and Meijer (2013)
Saturation concentration (kg/m^3)	5.25	271.1	Leeder (1999), Topper and Meijer (2013)
Area covered by deposit (m^2)	5.33E+9	6.65E+8	This work
Volume in CMD (m^3)	3.80E+11	9.63E+10	This work
Erosion rate (mm/a)	From 0.20[a] up to 3.16[b]	0.5–0.75[c] (for 50 mm/a precipitation) 20[d] (for 100 mm/a rainfall)	[a]Sanna et al. (2015) [b]Calaforra et al. (1993) [c]Frumkin (1994) [d]Mottershead et al. (2005)
Precipitation rate (mm/a)	1[a]–100[b]	100[c,d]–150[e]	[a]Orti Cabo et al. (1984) [b]Schreiber and Hsü (1980) [c]Lensky et al. (2005) [d]Sirota et al. (2018) [e]Manzi et al. (2012)

Note: Erosion rates are not used in the modelling but are used for considerations in the discussion.

$$S(t) = \frac{m_{\text{salt}}}{V_0 - \text{fwb} * t} \tag{4}$$

Where m_{salt} is the mass of salt [kg] contained in the basin at the start of drawdown (i.e., upon disconnection) and V_0 the initial volume of the basin [m^3].

During at least part of its MSC evolution, the CMD is likely to also have been subject to saline water fluxes through its connections. This means that the concentration of ions would have changed while the water volume stayed the same. For a basin with a negative freshwater budget that is fully balanced by a saline inflow (Figure 4b), the concentration of dissolved ions, and hence the salinity, increases over time. If either gypsum or halite reaches its saturation concentration in the process, the mass that exceeds this threshold concentration is taken to be precipitated as a uniform layer without getting re-dissolved. In the following we use $\Gamma = \frac{m_{\text{prec}}}{t}$ [kg/s] to describe the rate at which mass is precipitated. It is important to note that salinity can increase past the point at which precipitation begins since the ion group of the other salts can continue to concentrate (Equation 1). In that scenario the evolution of salinity S with time t is dependent on the magnitude of the influx Q_{in} and its salinity S_{in}

$$S(t) = S_0 + \frac{Q_{\text{in}} * S_{\text{in}} - \Gamma}{V_0} * t \tag{5}$$

For a basin like the CMD, it is likely that the exchange through the two sections is more complex than only inflow to balance the freshwater budget. By assuming that the salinity of the inflow through the northern connection is the same or close to the salinity of the inflow through the southern connection, we can simplify the system by combining these two fluxes to one inwards flux. The same applies to the fluxes leaving the basin through the two connections (Figure 4c). In this scenario, the salinity of the basin, S_{out}, is dependent on the properties of these combined in- and outflows respectively.

$$S(t) = S_0 + \frac{Q_{\text{in}} * S_{\text{in}} - Q_{\text{out}} * S_{\text{out}} - \Gamma}{V_0} * t \tag{6}$$

A special case to consider is the situation where neither salinity nor water volume of the basin change in a system of this kind. These two conditions can be described as $\frac{dV(t)}{dt} = 0$ and $\frac{dS(t)}{dt} = 0$ and lead to two expressions

$$Q_{\text{in}} = Q_{\text{out}} + \text{fwb} \tag{7a}$$

$$Q_{\text{in}} * S_{\text{in}} = Q_{\text{out}} * S_{\text{out}} + \Gamma \tag{7b}$$

For the special case without precipitation ($\Gamma = 0$), these two can be combined in a way that allows us to calculate the fluxes that would be needed to attain a certain salinity ratio (Knudsen, 1900),

$$Q_{\text{out}} = \frac{\text{fwb}}{\frac{S_{\text{out}}}{S_{\text{in}}} - 1} \text{ and } Q_{\text{in}} = \frac{\text{fwb}}{1 - \frac{S_{\text{in}}}{S_{\text{out}}}} \tag{8}$$

If the basin has already reached saturation, Γ will become non-zero and must be considered. There are scenarios for which we can calculate values for Γ as a function of other parameters of the system. The simplest case is a scenario in which both the in- and the outflow are saturated in a salt, either gypsum or halite. While the salinity can increase, the concentration of the salt in question cannot, leading to the precipitation of the excessive mass. Applying Equations (7a) and (7b) to only the concentration of a single salt for a

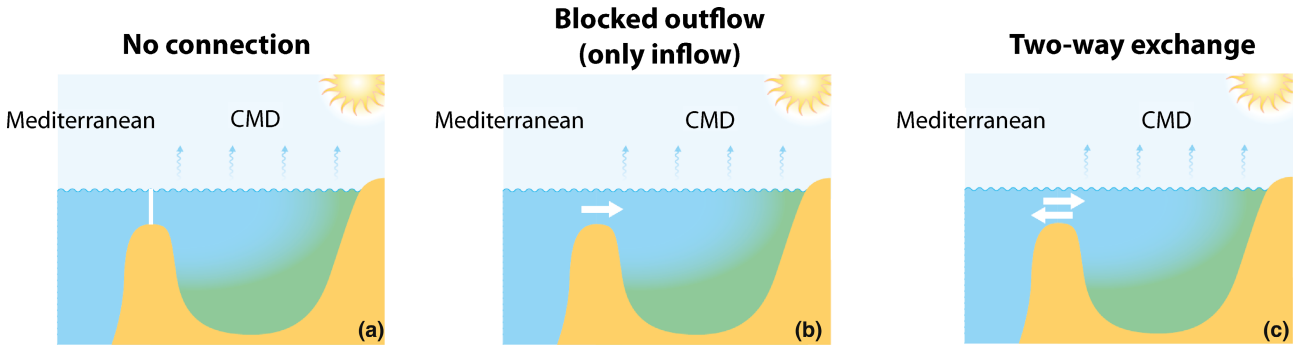

FIGURE 4 Different ways to approach the connection between the CMD and the open Mediterranean. (a) No connection between the CMD and the Mediterranean and thus both influx and outflux are cut. (b) The basin is connected to the open Mediterranean in a way that inflow compensates the loss of freshwater due to evaporation. (c) There is a two-way exchange over the sill. The inflow now compensates the freshwater budget as well as the saline outflow. Those three 'approaches' should not be conflated with the 'scenarios' that we present and discuss in the text, as they are strictly theoretical.

system in balance gives an expression for the precipitation rate in that special case. We thus have,

$$c[\text{salt}]_{\text{in}} = c[\text{salt}]^{\text{sat}} \text{ and } c[\text{salt}]_{\text{out}} = c[\text{salt}]^{\text{sat}}$$

with which Equation (7b) yields,

$$\Gamma_{\text{salt}} = \left(Q_{\text{in}} - Q_{\text{out}}\right) * c[\text{salt}]^{\text{sat}}$$

Combined with Equation (7a) we find,

$$\Gamma_{\text{salt}} = \text{fwb} * c[\text{salt}]^{\text{sat}} \tag{9}$$

For a more realistic scenario, where the inflow is below saturation while the basin has reached that threshold, the number of unknowns increases, and the precipitation becomes dependent on the magnitude of the outflux and the concentration of the influx The conditions for the concentrations can now be written as

$$c_{\text{in}} < c[\text{salt}]^{\text{sat}} \text{ and } c[\text{salt}]_{\text{out}} = c[\text{salt}]^{\text{sat}}$$

Inserting those conditions into Equation (7b) and substituting Q_{in} again with Equation (7a) gives

$$\Gamma_{\text{salt}} = Q_{\text{out}} c_{\text{in}} + \text{fwb} * c_{\text{in}} - Q_{\text{out}} * c[\text{salt}]^{\text{sat}}$$

Which can be rewritten in a way to express it in dependence of the ratio between the concentrations of the in- and outflow

$$\Gamma_{\text{salt}} = c[\text{salt}]_{\text{in}} * \left(Q_{\text{out}} * \left(1 - \frac{c[\text{salt}]^{\text{sat}}}{c[\text{salt}]_{\text{in}}}\right) + \text{fwb}\right) \tag{10}$$

With Equation (10) it is now possible to explore the rate of precipitation for a set of scenarios that are not only defined by their fwb but also by Q_{out} and c_{in}. To compare the results of Equations (9) and (10) with literature values they need to be expressed as rate of sedimentation (i.e., thickness of deposit per unit of time rather than mass). For this we need the density of the deposit, ρ_{deposit} (Table 2), and the area, A_{deposit}, covered by the deposit of interest. It is then also possible to calculate the duration of the period of deposition for each Γ, from an observed volume of the deposit,

$$T_{\text{prec}} = \frac{V_{\text{deposit}} * \rho_{\text{deposit}}}{\Gamma_{\text{salt}}} \tag{11}$$

Applying Equation (11) to the total volume of the deposit gives the total timespan during which this salt would need to precipitate at a given rate to form the observed deposit. To get the average duration of precipitation per precessional cycle (23 kyr), the volume needs to be divided by the number of total cycles during which it formed.

It is worth noting that the depositional process used in our modelling is purely evaporative and does not take into consideration more complex bio-geochemical processes that might have played a role in the PLG formation, at least locally where low salinity values were obtained from water inclusions in PLG gypsum crystals (e.g., Piedmont Basin, Italy; Natalicchio et al., 2014; Calabria, Italy; Costanzo et al., 2019), although the reliability of the salinities obtained from fluid inclusions measurements was recently questioned (Bigi et al., 2022). With the modelling approach presented here, we also do not take the influence of erosion into account.

4 | RESULTS

In this section, we apply the theory as described in Section 3.2 to the data that were presented in Section 3.1 to identify the key processes that are needed to explain the MSC deposits in the CMD. We find that a saline flow into as well as out of the CMD is needed to form the gypsum deposit, while the halite deposit could have formed from a disconnected CMD filled with saturated brine undergoing a water level drop.

4.1 | Water and evaporites volume considerations

As a first step, we calculate the volumes of water required to precipitate the observed volume of evaporites, V_G for gypsum and V_H for halite, and compare these with the (reconstructed) volume of the CMD. This will allow us to judge whether the evaporites could have formed by concentration of the water contained within the CMD or whether an additional influx of water and salt must be invoked.

For a range of water volumes (m^3) representing the CMD at a given water level, we calculate the concentration (kg/m^3) the water would attain if the mass of the observed evaporite (in kg) was dissolved in it. If the calculated concentration is lower than the concentration at which the water is saturated in the salts ($CaSO_4$, gypsum; NaCl, halite), then the water volume is big enough to hold the volume of the evaporite in a dissolved state. The minimal volume of water needed is determined as the volume at which the calculated concentration equals halite or gypsum saturation and was defined by Equation (1) and can be calculated with data as listed in Table 2.

The results, depicted in Figure 5, show that for the halite deposit this minimal water volume $V_{\text{min}} = \frac{9.633 * 10^{10}\ \text{m}^3 * 2200\ \text{kg/m}^3}{272.1\ \text{kg/m}^3} \approx 780\ \text{km}^3$ which is about equal to the capacity of the CMD below the level of the sill

lying at −850 m (sill 01 in Figure 3). If instead we take the observed mass of halite and assume this to be dissolved in the volume of water comprised by the CMD below each horizontal level (i.e., water level below 0; Figure 5), we find the basin water to attain saturation values once the level is lowered to the depth of the sills (orange line in Figure 5). This is of course consistent with the V_{min} calculation and confirms its result.

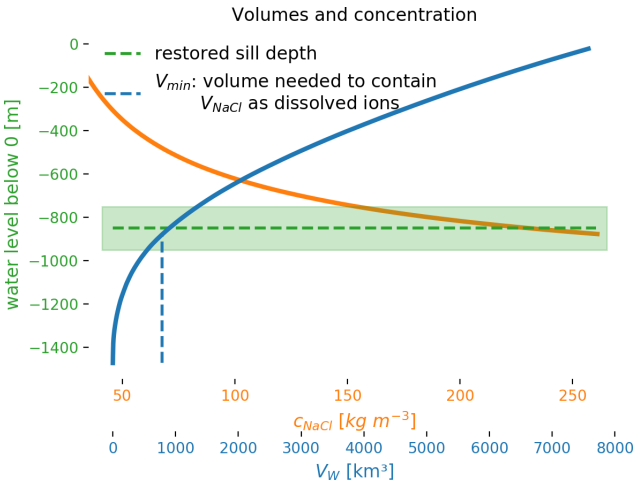

FIGURE 5 With water level on the vertical axis, the solid blue line gives the water volume of the pre-Messinian CMD below each level (see blue horizontal axis). The dashed green line depicts the level of the sills, with an uncertainty of ±50 m (green area). The water volume of the CMD below sill depth (i.e., at the crossing between the solid blue and dashed green lines) is about equal to the volume of halite-saturated water required to form the observed halite deposit (V_{min}) which is indicated with the vertical blue dashed line. Also shown as a function of water level is the concentration that the basin waters would attain if the observed mass of halite was dissolved in it (solid orange line and orange horizontal axis). Since the volume of water decreases with a lower water level, the resulting concentration increases until it reaches $c[NaCl]^{sat} = 271\ kg/m^3$ at a depth of −879 m, which corresponds to a water volume of $V_{min} = 780\ km^3$ (see text for details).

In a similar type of calculation, we take the volume of water comprised by the basin at sill depth (Table 3) and assume saturation concentration of gypsum and halite, respectively. This way we compute the maximum volume of gypsum or halite that can be precipitated from a disconnected basin. These calculations show that only a fraction of the observed gypsum volume (0.9%) of the BU1/2 (Table 1) could precipitate from the water volume available below sill depth, while more than 100% of the observed halite volume could be stored in the basin volume below the sill.

The results indicate that the gypsum deposit is too massive to originate from a disconnected basin, even if it was saturated in gypsum, while the halite deposit could have precipitated from a disconnected basin saturated in halite (Table 4). The calculation does not inform us about the timespan over which the halite deposit was formed. This can be determined by the time it would take until a disconnected CMD would reach a new equilibrium between river inflow and net evaporation, which is addressed in the next section (Section 4.2).

4.2 | Desiccation of an isolated basin

The only realistic process that could isolate the CMD is a water level drop in the Mediterranean Sea that lowers the level of the surrounding waters below the level of the sills. Bringing the level below that sill would cancel the exchange of saline water through the connections and the later evolution of the CMD would be independent of the rest of the sea. In this section, we investigate such a scenario (Figure 4a).

For such an isolated basin, the new balance is described by the fwb, as defined in Equation (3) and thus dependent on the river influx R and loss of water to the atmosphere $(E-P)*A$. As long as more water is lost than added, the CMD experiences a drawdown that is not

TABLE 3 Morphometric parameters of the study area used as input for our modelling

	CMD	Valencia Basin	References
Present-day area (m^2)	11.83E+9	57.60E+9	This work
Maximum paleo-depth (m)	1500	1800	Heida et al. (2021)
Sills paleo-depth (m)	Sill02 = 700 Sill01 = 850	No sill (open basin)	This work
River inflow (m^3/s)	≤10[a] Present-day	500[b] Paleo	[a]Garcia et al. (2017) [b]Urgeles et al. (2011)
Evaporation rate (m/a)[b] (for the model)[1]	0.25–1.5[a] 1.04[b]	0.25–1.5[a]	[a]Estrany et al. (2011) [b]Simon and Meijer (2017)
Strait parameter g (m^3/s/sqrt(kg/m^3))	10^5 Present-day	–	Barceló-Llull et al. (2019)

[1]Evaporation rates are present-day values (Estrany et al., 2011; Simon & Meijer, 2017) assumed to be similar to those during the MSC.

TABLE 4 The maximal volumes of gypsum and halite that can be precipitated from the CMD as a disconnected basin

Unit	Percentage of observed volume that can be precipitated from a CMD filled to the sill (−850 m) with water at saturation
BU1/2	0.9% (1.1%)
BU3	2.2% (2.8%)
BU1/2 + BU3	0.6% (0.7%)
Halite	141% (170%)

Note: The calculations use the available water volume below sill depth at −850 m and −800 m according to pre-MSC hypsometry and saturation concentration for Gypsum (145 kg/m^3) and Halite (350 kg/m^3). For each deposit or combinations of deposits, the volume of water in the basin is adjusted to account for the predating deposits that occupies accommodation space.

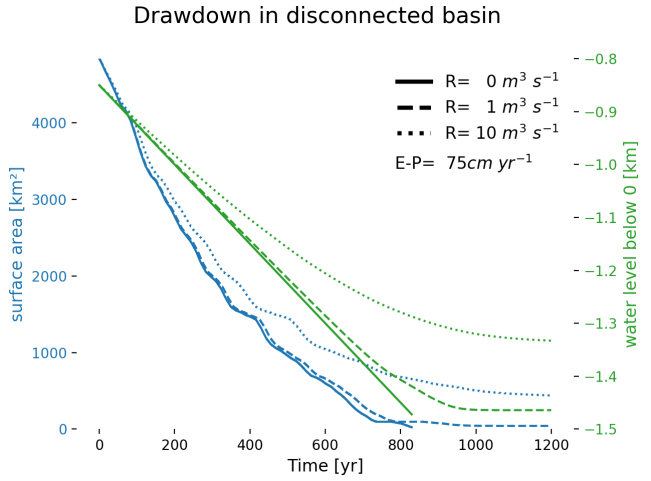

FIGURE 6 Desiccation of the CMD. This figure shows the change over time in water level (green) and surface area (blue) for three different strengths of river inflow, R [m^3/s] for a disconnected basin at a given net evaporation, $E-P$ [cm/yr]. As soon as the CMD is disconnected from the surrounding waters, the negative freshwater budget causes the water level to fall further below the sill depth (850 m). The basin only desiccates completely if there is no inflow from rivers (solid lines), for non-zero values of R (dashed, dotted) the system will reach a balance where it loses as much through evaporation as it gains by river input.

dependent on the drawdown of the Mediterranean Sea. This process changes the surface area that is available for net evaporation and continues until a new stable state is reached where the flux to the atmosphere is of the same size as the river inflow, which may, to first approximation, be considered constant. These two fluxes thus determine the water level in the new steady state that is defined by fwb = 0 (Equation 3), as well as the time needed to reach it. The results are depicted in Figure 6, which shows that the timespan on which the process takes place is less than 1 kyr. The fastest change occurs in an extreme scenario without any river input at all (solid lines). In that case, the steady state of a completely desiccated basin is reached after less than 900 yr. A river input of $R = 1\,m^3/s$ is close to the present-day situation (Garcia et al., 2017) and would lead to a stable state after less than 1000 yr (dashed lines). In contrast to the first scenario, the basin would not completely desiccate, and the remaining water would have a depth of 8 m. A ten times higher river input of $R = 10\,m^3/s$ leads to a larger remaining volume and a remaining water depth of 140 m. In theory there is also a corresponding river influx R for each net evaporation $(E-P)*A$, and vice versa, that would prevent a drawdown for the disconnected basin, i.e., fwb = 0 for a basin with its surface at sill depth. To achieve this, a net evaporation of 0.75 m/yr would have to be balanced by an unrealistically high influx of 340 m^3/s, while inversely, the more realistic influx of 1 m^3/s (Table 3; Garcia et al., 2017) would require a net evaporation as low as 0.002 m/yr. Both combinations are unrealistic, which implies that a disconnected CMD would experience a drawdown, until the surface area is small enough for the river inflow to balance the net evaporation. The loss of freshwater during that time would lead to an increase in salinity because the dissolved ions stay in the system.

In the previous section (Section 4.1), simply looking at volumes, it was argued that the halite deposit could have formed from a situation where the CMD was already at, or close to, halite saturation at the moment of disconnection. In that case, the water within the CMD would become oversaturated during a drawdown leading to the precipitation of the surplus ions (Equation 4). However, it follows from the reasoning in the current section that the resulting halite deposit will be smaller in mass and volume than the observed one, since the inflow from rivers prevents a complete desiccation. For a scenario with a high river inflow of $R = 10\,m^3/s$ only 2.3% percent of the initial water volume remains in the basin and since a disconnected CMD at halite saturation could precipitate 144% of the observed halite volume, this effect is small enough to be ignored.

The question yet to be answered is if and how the CMD could reach halite saturation before it was disconnected.

4.3 | Full basin, inflow only

To understand if it is possible that the CMD reached halite saturation before the end of Stage 1 (i.e., the end of gypsum deposition), we consider the fastest change in concentration possible for a basin with constant volume (Equation 5). The same is applied to the Valencia Basin, which allows us to compare the behaviour of the two basins.

For this scenario, we will not assume a drawdown but keep the water level steady at 0 m. To preserve volume, all water lost to the atmosphere is replaced by saline water that is flowing into the basins from the open Mediterranean (Figure 4b). This process adds ions to the water volume of the basins which can only be removed by precipitation, since there is no saline outflux. Unless $fwb = (E - P) * A - R < 0$, the salinity will increase (Figure 7). The rate of this increase is dependent on the fwb, the water volume of the basin as well as the salinity S_0 of the inflow. Since S_0 is the same for the CMD and the VB, the difference in the rate of change between the CMD and VB is dependent on the ratio between their volume and the corresponding fwb. The latter is also dependent on the surface area of the basin in question (Table 3). We find that for the VB, the net evaporation needed to balance a realistic river inflow is 0.27 m/yr, which is 100 times higher than for the CMD. The much larger volume of the VB explains why this basin experiences a different rate of salinity increase for the same net evaporation rate $E - P$ even when, for the CMD, a very high river input (10 m^3/s instead of ca. 1 m^3/s taken from Garcia et al., 2017; Table 3) is chosen (Figure 7). The slow salinification of the VB in comparison with the CMD even for higher values of $E - P$ might be an indicator that the salinity of the VB was lower than the one of the CMD.

Focusing on the CMD, it follows from Figure 7 (see also Table 5) that the time needed to form the observed halite deposit, $T[\mathrm{NaCl}]_{vol}$, is short enough for this to have happened during Stage 2 (ca. 50 kyr). The same applies to the time needed to reach halite saturation, $T[\mathrm{NaCl}]_{sat}$. With $T[\mathrm{NaCl}]_{sat} = 21$ kyr for the slowest scenario tested, this time span is shorter than the duration of Stage 1, meaning that the basin would have reached halite saturation even before the beginning of Stage 2. However, $T[\mathrm{NaCl}]_{sat}$ is much shorter than the time needed to precipitate the gypsum of BU1/2, i.e., duration $T\left[\mathrm{CaSO_4}\right]_{vol}$. This means that in this scenario the basin would reach halite saturation before the observed volume of the gypsum deposit could be precipitated, which indicates that the inflow-only scenario is incompatible with the observed presence of gypsum and halite.

To find out whether there is a set-up where halite saturation is reached only after the full volume of the BU1/2 has been deposited, $T[\mathrm{NaCl}]_{sat}$ as described in Equation (5) must be equal to $T\left[\mathrm{CaSO_4}\right]_{vol}$ which can be derived from Equation (10). This leaves us with an expression which is not dependent of the fwb and shows that for an inflow salinity of $S_0 = 35.05\ \mathrm{kg/m^3}$ the volume of the CMD would have to be 8.3 times larger than its volume at normal sea level. This again indicates that the gypsum

TABLE 5 Comparison of the time the CMD would need to deposit the gypsum deposit $\left(T\left[\mathrm{CaSO_4}\right]_{vol}\right)$ or halite deposit $\left(T[\mathrm{NaCl}]_{vol}\right)$ compared with the time it would reach halite saturation $\left(T[\mathrm{NaCl}]_{sat}\right)$ for the same conditions and the scenario as described in Figure 7 and shown in Figure 4b

S_{in} (kg/m^3)	$E-P$ (m/yr)	$T\left[\mathrm{CaSO_4}\right]_{vol}$ (kyr)	$T[\mathrm{NaCl}]_{sat}$ (kyr)	$T[\mathrm{NaCl}]_{vol}$ (kyr)
37	25	182	21	0.62
145	75	15	1	0.16

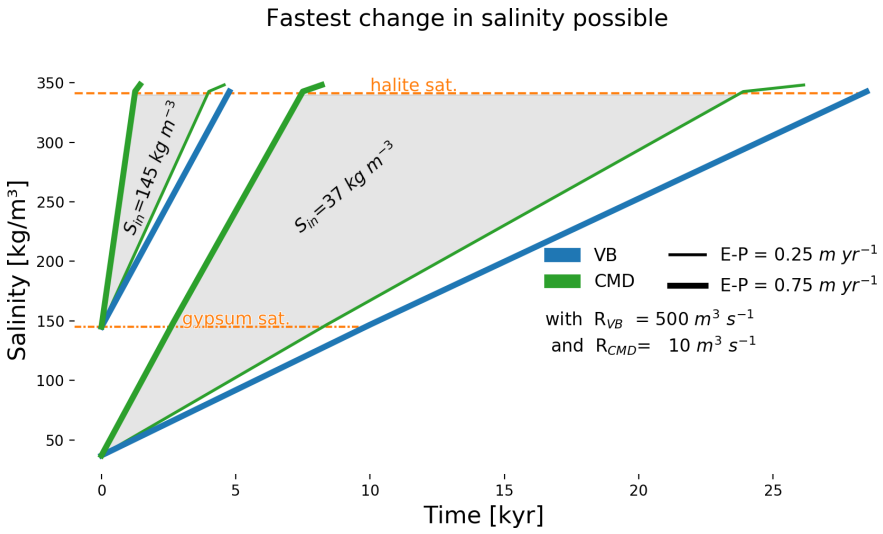

FIGURE 7 Fastest change in salinity possible for CMD and Valencia Basin (VB). All fresh water that is removed from the system due to fwb >0 is replaced by saline water representing an inflow. No saline outflow is applied. The increase in salinity is shown for the CMD (green lines) and VB (blue lines) for two different inflow salinities (Sin = 37 kg/m^3; Sin = 145 kg/m^3) as well as for two different net evaporation rates ($E - P = 0.25$ m/yr, thin lines; EP = 0.75 m/yr, thick lines). The grey swaths filling the space between the thick and the thin green line resemble the family of functions with the same S_{in} but varying fwb.

and halite cannot have formed by the same mechanism (i.e., blocked outflow). It is likely that the formation of the gypsum deposit requires a more complex mechanism than the one considered here. A saline outflow would not only keep the salinity from quickly rising to halite saturation values but would also be more realistic for a basin with two wide connections to surrounding waters.

4.4 | Two-way exchange

The presence of an outflow from the CMD to the surrounding western Mediterranean would have allowed the CMD to maintain a salinity in the range of gypsum saturation for a longer period of time than in a blocked outflow scenario. To explore this new scenario, we now quantify the size of the volume flux of water out of the basin for the case that the basin stabilizes just below gypsum saturation, while maintaining constant volume. Let us consider the two extremes of the mathematical solution, a non-existent and an infinite outflow. The first, a non-existent outflow, would lead to the situation described in Figure 7, with ever-increasing salinity. In the second extreme, the salinity of the basin would be the same as that of the inflow. In between these two extremes there exists an outflow strength for every inflow salinity such that the basin maintains gypsum saturation. If the outflow is larger than the calculated value, gypsum saturation will not be reached. We thus compute the maximal outflux that would still allow for gypsum saturation. The absolute value of this maximal outflux as given by Equation (8) and is dependent on the salinity of the inflow as well as the fwb of the basin. The latter is defined by a given $E - P$, the surface area as well as a river inflow which is set to $R = 2\ \mathrm{m}^3/\mathrm{s}$.

The results of this calculation are shown in Figure 8 as a function of the inflow salinity and the level of the water surface. The three swaths represent families of curves that describe a range of $E - P$ and are defined by a given outflow strength. Swaths corresponding to a relatively large outflow sit at higher inflow salinity, since with relatively large exchange the basin salinity is close to that of the adjacent water. If the basin is to attain gypsum saturation, the salinity of the inflow must already be close to that.

For a given value of the outflow, i.e., within a given swath in Figure 8, the curves shift towards higher inflow salinity for lower $E - P$, with the lowest $E - P$ defining the right-hand border of the swath. When $E - P$ is small, fwb is small, the inflow thus exceeds the outflow by a smaller amount (Equation 7a) and its salinity must be higher to still achieve saturation. The slope of the curves towards the right in Figure 8, i.e., the shift to higher inflow salinity for lower water level, is explained by the same mechanism. The change in fwb is in that case caused by the decrease

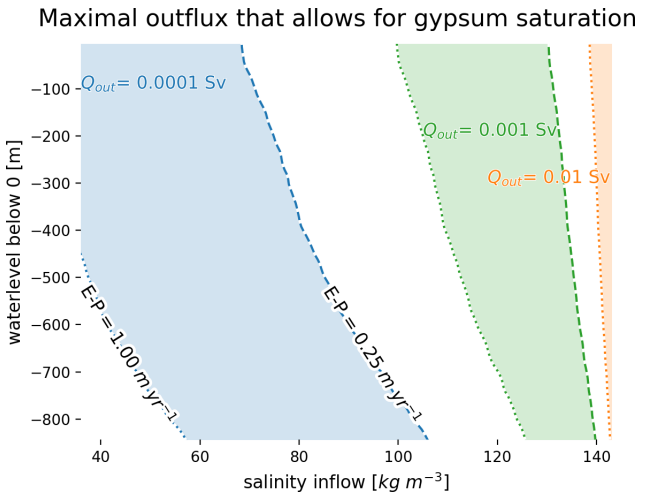

FIGURE 8 Model estimation of the precipitation of gypsum in the CMD as a function of water level and salinity in the Mediterranean, and the magnitude of the water flow into the CMD. With two-way flow across the sills that connect it to the western Mediterranean, the CMD will reach a constant salinity. This graph illustrates the conditions under which the CMD stabilizes exactly at gypsum saturation (calculated with Equation 8). Each coloured swath corresponds to a certain magnitude of the outflow and comprises the curves obtained for a range of values of $E - P$, as indicated. The swaths are plotted as a function of inflow salinity on the horizontal axis. The vertical axis gives the level of the water surface: since the area subject to evaporation becomes less upon drawdown, the water level together with $E - P$ determines fwb. The path for $Q_{\mathrm{out}} = 0.1$ Sv is too thin to be properly displayed in this figure and would be located in a narrow band close to an inflow salinity of $145\ \mathrm{kg/m^3}$.

in surface area for lower water levels. Thus, a given $E - P$ then corresponds to a smaller fwb and less net input of salt to the basin. Comparison of the fwb for a water level at sea level with a water level at the depth of the sills (-850 m) shows a decrease of about 50% (e.g., $E - P = 0.25\ \mathrm{m/yr}$, $R = 10\ \mathrm{m}^3/\mathrm{s}$, decrease = 53%). The influence of drawdown is thus smaller than one order of magnitude.

For low inflow salinities, the fluxes needed for the basin to reach gypsum saturation ($S_{in} < 80\ \mathrm{kg/m^3}$) are several orders of magnitude smaller than the ones that are measured today (ca. 0.1 Sv; Barceló-Llull et al., 2019). This means that in a situation where the inflow salinity is less than $140\ \mathrm{kg/m^3}$ the fluxes to and from the basin would need to decrease several orders of magnitude for the basin to stay at gypsum saturation, independently of drawdown and net evaporation. Without any external factors that decrease the magnitude of the fluxes, like a strong slowdown of the circulation, the only way for the CMD to reach gypsum saturation is when the salinity of the surface to intermediate layer of the Western Mediterranean Sea is already very close to saturation. The same applies to reaching halite saturation in the basin.

4.5 | Precipitation of gypsum

In the previous section (Section 4.4), we focused on the situation right before precipitation and the fluxes which would be needed to maintain this. We now calculate precipitation rates resulting from specific combinations of outflow, fwb and salinity of the inflow (Equation 9). To reduce the number of unknowns, we now look at a full basin and consider a single value for $E-P$. This is allowed since it is already known from previous calculations that a drawdown only has a minimal effect on the system (see Section 4.2). Net evaporation also has an influence, but just like drawdown, this influence is minor and does not change the overall behaviour of the system.

Based on Equations 9 and 10, we can calculate first the precipitation rate (Γ) and then the duration of precipitation that follows from this precipitation rate as being required to explain the observed volume of gypsum. The lower the precipitation rate, the longer it would take to precipitate the observed volume and for the mathematically correct but unrealistic solution this time span would tend to infinity. To avoid this type of solution the results are filtered to be within geologically realistic limits. From previous studies it is known that a realistic margin for the precipitation rate of gypsum ranges from 1 m/kyr (Orti Cabo et al., 1984) to 100 m/kyr (Schreiber & Hsü, 1980), while the duration of precipitation per precessional cycle cannot be longer than the length of the cycle itself (assumed to be 23 kyr).

The results are shown in Figure 9 (compare with Section 4.4; Figure 8). The grey line indicates the minimum inflow salinity that would lead to gypsum saturation for a given outflux strength. The higher the magnitude of the outflow, the higher the salinity of the inflow needs to be for the basin to reach gypsum saturation. Precipitation starts when this salinity (145 kg/m^3) is exceeded and the duration of precipitation itself ranges between 0.8 and 5 kyr per cycle and thus lasts between 5% and 20% of a precessional cycle. For lower magnitudes of outflow, for example, it becomes clear that the higher the inflow salinity is, the shorter the duration of precipitation per cycle. This can be explained by the increasing amount of excess ions that are transported into the basin for higher salinities. The same observation is valid for halite (Figure 10) and will be discussed in Section 5.2.

Another interesting aspect is that, the stronger the outflow through the connections is, the smaller the range of possible salinities that would lead to a realistic precipitation rate becomes. This means that knowing the actual strength of the fluxes would not only provide us with a range of inflow salinities and thus salinity of the upper layer of the Mediterranean Sea at that time, but also that the higher those fluxes are, the smaller the range of possible

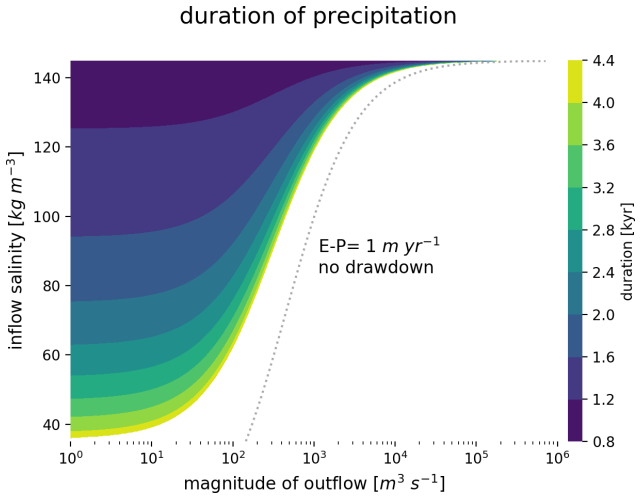

FIGURE 9 Duration of the period required to precipitate the observed volume of gypsum in the CMD, for different values of the outflow and the salinity of the inflow, when no drawdown is applied and $E-P = 1$ m/yr. The grey dotted line indicates the minimum inflow salinity that is needed for the CMD to reach gypsum saturation for a given outflow magnitude. For each pair of outflow strength (x-axis, logarithmic) and inflow salinity (y-axis, linear) the timespan per cycle that is needed to precipitate the observed gypsum volume of the BU1/2 is calculated. The results are clipped by limiting the rate of precipitation rate to be between $1\,\mathrm{m/kyr} < \Gamma < 100\,\mathrm{m/kyr}$.

salinities is. While for an outflux of $Q_{out} = 10\,\mathrm{m^3/s}$ an inflow salinity of $\left[40\,\mathrm{kg/m^3},\ 145\,\mathrm{kg/m^3}\right]$ could lead to the observed BU1/2, this range would be limited to $[144\,\mathrm{kg/m^3}, 145\,\mathrm{kg/m^3}]$ for $Q_{\mathrm{out}} = 10^5\,\mathrm{m^3/s}$. The latter is close to the strength that is measured today (Barceló-Llull et al., 2019).

5 | DISCUSSION

In this section, we discuss the significance of our results on the MSC events in the CMD and in the Western Mediterranean. Section 5.1 focuses on the first stage of the MSC, known also as the PLG stage (5.97–5.60 Ma). The main outcome from Section 5.1 is that during stage 1 of the MSC, the salinity of the upper water layer of the Western Mediterranean reached gypsum saturation for relatively 'brief' periods of precessional cycles, and provided the CMD with the necessary Ca^{2+} and SO_4^{2-} ions to deposit the observed gypsum volume through a two-way exchange of fluxes.

Section 5.2 focuses on stage 2 of the MSC (5.60–5.55 Ma). The main crucial conclusion in this sub-section is that the only way possible to deposit the observed halite volume in the CMD during this stage is a scenario in which it is disconnected from the open Mediterranean. This requires a high amplitude base-level drawdown of at

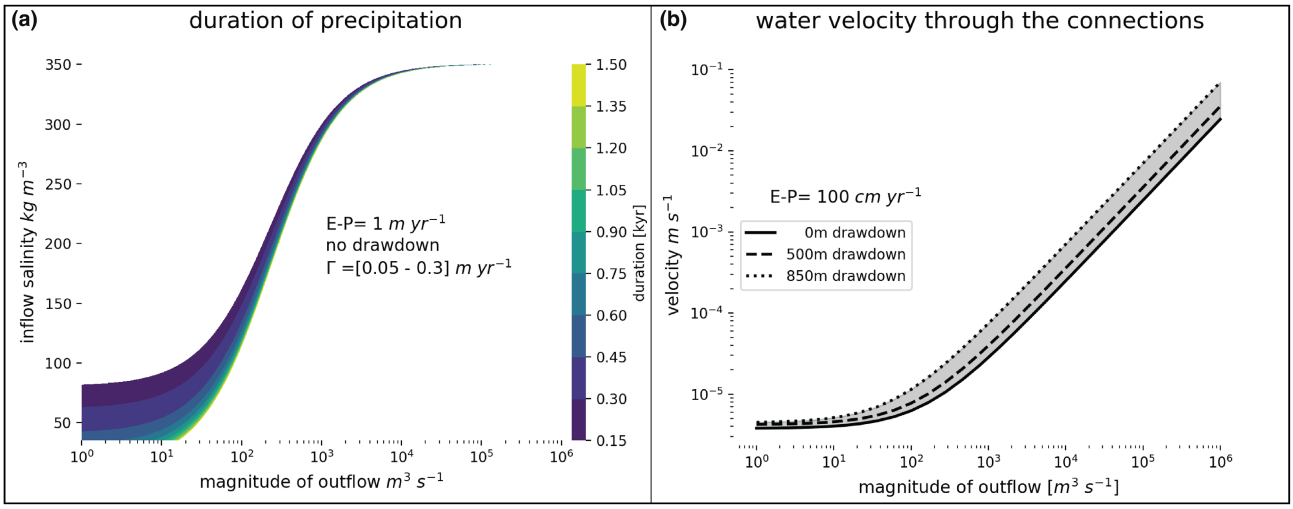

FIGURE 10 (a) Duration of precipitation for the halite deposit in analogy to Figure 9. The boundaries for the precipitation rate are oriented at those of the Dead Sea (Table 2), with ±2 order of magnitudes to cover broader boundaries. (b) Velocity of water fluxes through the connection in dependence of drawdown and magnitude of outflow.

least ca. 850 m, in which halite saturation is reached both in the CMD and in the Western Mediterranean only when the water level was significantly lowered (Figure 11).

5.1 | The pre-halite lower gypsum in the CMD: Stage 1 of the MSC

The pre-Halite MSC units of the CMD (BU1 and BU2) are interpreted as Lower Gypsum belonging to stage 1 of the MSC (Table 1; see Section 2.3 and Raad et al., 2021). The estimated volume of the evaporitic gypsum content of both units is ca. $3 \times 10^{+11}$ m^3. Due to estimation uncertainties, related mainly to the limited seismic coverage in some parts of the CMD (Figure 2) and assumptions on the internal lithology of BU1 and BU2, there is a chance that this volume has been slightly underestimated, but this would not change the following line of reasoning which is based on qualitative results. Even an underestimation of 30% of the gypsum volume would only have a noticeable influence on the duration of precipitation, changing the interval from 5%– 20% to 6.5%–20%.

Our results show that the volume of pre-halite gypsum observed in the CMD (Table 1) is too high to precipitate from a disconnected basin scenario. A CMD filled with water at gypsum saturation concentration (145 kg/m^3) up to the sill depth would produce a volume of gypsum that is far too small with respect to the observed volume (0.9%; Table 4). This implies that if the CMD was ever disconnected from the surrounding waters, gypsum should have started deposition before the disconnection happened, i.e., when the CMD was still supplied with an input of Ca^{2+} and SO_4^{2-} ions. In this case, two possible

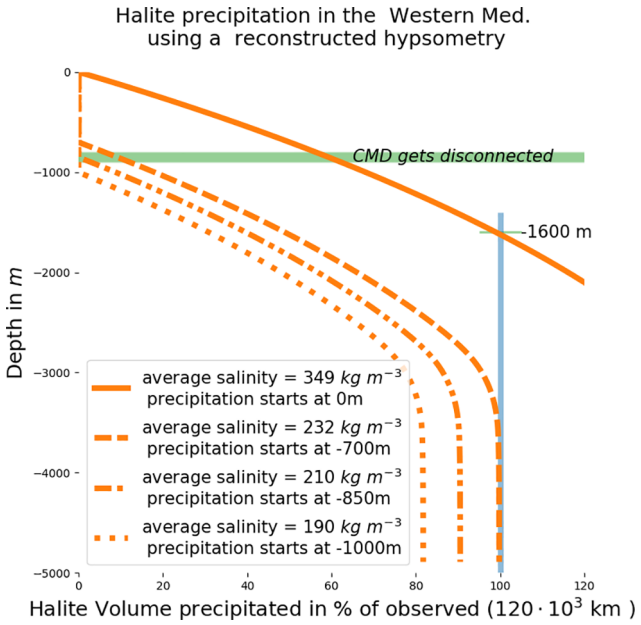

FIGURE 11 Halite volume that would form from a drawdown in the Western Mediterranean. The orange lines show the precipitated volume of halite in function of the amplitude of the drawdown. The shape of the curves is determined by the hypsometry of the basin and the average salinities of the water column before drawdown. Once the drawdown is progressed, the water volume of the basin is decreased enough so that it reaches halite saturation and precipitation begins. The green bar indicates the depth at which the CMD would have become disconnected, and the thin green line marks the depth at which the full deposit would have formed from a full water column at halite saturation.

scenarios can be considered: (1) A basin with only an influx from the surrounding Mediterranean waters into the CMD without an outflux; (2) A CMD with 2-way

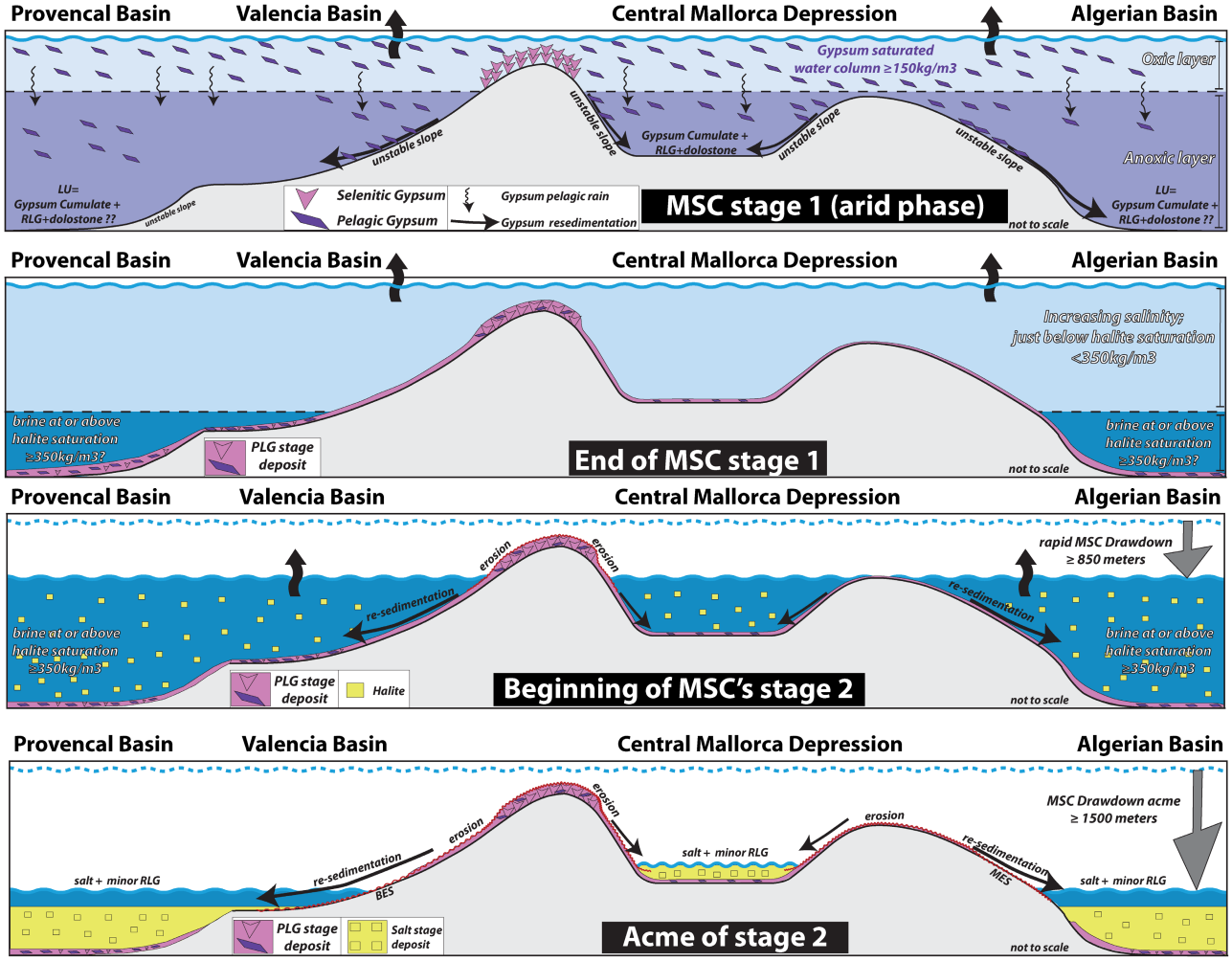

FIGURE 12 Schematic representation of the depositional conditions in the Western Mediterranean during stages 1 and 2 of the MSC according to our modelling results. The non-silled Valencia Basin does not feature the presence of Halite on seismic dataset in its present-day setting (Maillard et al., 2006). Erosion rates measured in exposed halite can be as high as 20 mm/yr (Frumkin, 1994; Mottershead et al., 2005), suggesting that halite was subsequently removed towards the deeper Provencal Basin following the acme of the drawdown (Heida et al., 2021).

fluxes from and into the surrounding Mediterranean waters. For the first case (1), our results presented in Figure 7 show that even in the slowest possible scenario ($E - P = 0.25$ m/yr), the salinity of the CMD would increase very rapidly jumping to gypsum saturation in about 7 kyr and continuing to halite saturation concentration in 21 kyr, thus not allowing enough time for the observed gypsum volume to precipitate ($T\left[\mathrm{CaSO_4}\right]_{\mathrm{vol}} = 182$ kyr; Table 5). In the second case (2), a saline outflux would slow down the rapid salinity increase in the CMD giving longer timespans for the gypsum to precipitate. Figure 8 shows that in this scenario, for the CMD to stabilize at gypsum saturation, the saline influx should be very close to if not exactly at gypsum saturation concentration (between 140 and 145 kg/m^3; Figure 8) for an outflux which is equal to or one order of magnitude less than the one measured today across the silled channels (0.1 and 0.01 Sv, respectively; Figure 8). This is mainly due to the small volume of the CMD compared with its large connection to the surrounding waters (Figure 3) through the wide and deep channels, which maintains the salinity of the CMD equal to the salinity of the upper layer of the Mediterranean waters. Unless a drastic decrease in the fluxes caused by a more sluggish circulation (e.g., slowdown of the currents due to a base-level drop) of the Mediterranean currents took place, the CMD will have had almost the same salinity as the upper Mediterranean water layer, as is true for the present-day situation (Barceló-Llull et al., 2019). To our knowledge, until present, no studies showed or quantified such a decrease in the Mediterranean currents and its consequences during the MSC. Our calculations also show that gypsum precipitation could not have persisted for the whole duration of a precessional cycle. Instead,

the duration of gypsum deposition is restricted to 5% to 20% (i.e., 0.8–4.4 kyr/23 kyr) of a precessional cycle (Figure 9).

Our inferences have several important implications for what might have happened in the Mediterranean during stage 1 of the MSC. One important implication is that the saturation concentration of gypsum must have been reached in the upper layers of the open Western Mediterranean (Figure 12), at least during the dry periods of precessional cycles (i.e., insolation minima). Several studies showed that, due to the negative fresh water budget that characterizes the Mediterranean Basin, a reduction of the strait efficiency in the proximity of Gibraltar would lead to a drastic increase of the salinity of the Mediterranean waters (Blanc, 2006; Meijer, 2021; Meijer & Krijgsman, 2005; Topper & Meijer, 2013). The drop in diversity until the complete disappearance of planktic foraminifera in the Mediterranean during summer insolation minima, is, for example, one indication that surface waters reached salinities above the maximum tolerance of these organisms (Blanc-Valleron et al., 2002; Bulian et al., 2021; Sierro et al., 1999, 2003). One might argue that the salinity tolerance of planktic foraminifera generally does not exceed 50 kg/m^3 (Bijma et al., 1990), meaning that salinities in the Mediterranean water column did not necessarily reach gypsum saturation. This might be true for most of the duration of each precessional cycle of stage 1, but salinity probably peaked reaching gypsum saturation during relatively short timespans (Figure 9). Indeed, Topper and Meijer (2015) showed that the salinity of the open Mediterranean waters could rise to gypsum saturation, following a restriction with the Atlantic Ocean, in timespans that are as fast as 3 kyr.

Our result, thus, contradicts what has been proposed by Lugli et al. (2010) who suggested that gypsum saturation concentration was reached only in silled marginal basins whose salinity increase and the subsequent gypsum deposition was due to circulation restrictions imposed by the presence of the sill itself. This observation has been indeed also supported by Meijer (2021) who showed that in the case of a Mediterranean-marginal basin connection through sills, a strait efficiency as small as 10^3 m^3/s should occur in order for the marginal basins to reach gypsum saturation with a Mediterranean at normal salinity. This extremely low strait efficiency value is 'unrealistic' as it is in the order of magnitude of a large river flowing to the Mediterranean at present. Also De Lange and Krijgsman (2010) suggested that gypsum saturation and precipitation took place at all shallow-water depths when the upper Mediterranean waters were at gypsum saturation. In our opinion, the example of the CMD is an evidence that there is no need for a 'shallow' structural sill for gypsum to deposit. Most of the basins from which the shallow sill control idea comes from are basins now lying onshore and that underwent complex post-MSC tectonic evolution since the formation of the evaporites. Restoring their structural setting, including sill depths, at the MSC time is not straightforward and needs sophisticated tectonic reconstructions. Moreover, the few places in the offshore Western Mediterranean area where PLG was recovered in boreholes, are open shelves not or partially surrounded by sills (e.g., Alicante shelf and Valencia Basin; del Olmo, 2011; Ochoa et al., 2015; Soria et al., 2008; and offshore Western Algeria in the Arzew borehole; Burollet et al., 1978).

It follows that PLG could have been deposited almost everywhere in the Mediterranean Basin during stage 1, including open shelves (De Lange & Krijgsman, 2010; Krijgsman & Meijer, 2008), with probably selenitic gypsum dominating in the shallow oxygenated water layer and cumulatic gypsum below a certain water depth limited by the depth of anoxia level (Figure 12) (De Lange & Krijgsman, 2010; Dela Pierre et al., 2011; Natalicchio et al., 2021). In the CMD, this facies change could be marked by the passage from the MSC seismic unit BU1 to BU2 (Raad et al., 2021; see Section 2.3). In the deep basin, the so-called Lower Unit (LU) (Bache et al., 2009; Lofi et al., 2011; Montadert et al., 1978) could thus be the sediment resulting from this phase constituting of gypsum cumulates, clastic gypsum and dolostones (Figure 12). Local conditions such as high river inflow might have prevented gypsum formation by locally reducing the salinity (e.g., Ebro delta in the VB; Figure 7). Other local geo-chemical and geo-biological factors might have also prevented the formation of gypsum locally in deep basin context (e.g., reduced supply of gypsum from the water column and higher rates of bacterial sulphate reduction, deriving from permanent seafloor anoxia and larger availability of organic matter; Guibourdenche et al., 2022; Natalicchio et al., 2021). In shallow water where freshwater dilution did not play a role, the absence of PLG must mean that it has been removed after deposition. This removal of PLG could be due to two different causes. (1) It might have been redeposited into deeper settings due to gravitational instability (De Lange & Krijgsman, 2010). Such a process combined with local tectonic activity might be at the origin of the Resedimented Lower Gypsum (RLG) observed in some basins (Manzi, Roveri, et al., 2021; Roveri et al., 2006), but could have happened in any moment after the gypsum's deposition and not necessarily during stage 2 of the MSC (Figure 12), as also supported by observations from the MSC PLG in Cyprus by Artiaga et al. (2021); (2) It could have been the result of subaerial erosion during the main MSC water level drawdown

which amplitude has been recently revised to 1.5 km in the Western Mediterranean (Heida et al., 2021). Indeed, present-day denudation rates measured in gypsum (by denudation), including MSC gypsum from the Sorbas Basin (Calaforra et al., 1993; Sanna et al., 2015; Table 2), vary from low (0.20 mm/yr) to high (3.16 mm/yr). Such rates make it realistic to assume that even hundreds of metres of Gypsum could have been eroded during stages 2 and 3 of the MSC (total duration of ca. 270 kyr), during which the water level was lowered, and the shelves underwent intense erosion as attested by the Messinian Erosion Surface (Lofi et al., 2005, 2011; Urgeles et al., 2011). It remains unclear, however, why PLG is preserved only locally. Subaerial erosion and/or slope instability may have been more efficient on some margins compared with others.

Interpretation of stratigraphic and/or borehole data from onshore (Caltanissetta Basin, Manzi, Roveri, et al., 2021; Piedmont Basin, Dela Pierre et al., 2011) and offshore (Levant Basin, Manzi et al., 2018) 'intermediate to deep basins' contradicts the presence of gypsum in the distal domain of such basins, where the distal equivalent of stage 1 'marginal' PLG is represented by organic shales (Foraminifer Barren Interval, FBI; Manzi et al., 2018). This interpretation has been recently modified, at least for the Piedmont Basin, where Natalicchio et al. (2021) inferred the presence of Gypsiferous Mudstones in the distal domain of the basin. Regarding the deep Levant Basin, Meilijson et al. (2018) have already opposed such interpretation by putting the halite as stage 1 distal equivalent of the PLG. In addition, very recent XRD data from the deep Levant Basin's halite show important inclusions of calcium sulphates within the halite (Aloisi et al., in prep—personal communication).

The duration of gypsum sedimentation within a precessional cycle is also relevant. Lugli et al. (2010) suggested that time spans for gypsum formation within a precessional cycle could have been restricted to the peak of the aridity phase of the cycle (i.e., few thousands of years), which is in accordance with our calculations. Indeed, the relatively high deposition rates of gypsum (Table 2) compared with the low sedimentation rates of the terrigenous intercalations between consecutive gypsum beds (Lugli et al., 2010) makes it realistic that the sedimentation of the latter occupies most of the precessional cycles.

5.2 | Halite in the CMD: Stage 2 of the MSC

The salt unit of the CMD is interpreted as halite belonging to stage 2 of the MSC (Table 1; see Section 2.3 and Raad et al., 2021) and it has an estimated volume of ca. $9.63 \times 10^{+10}$ m^3. The seismic data coverage imaging the halite in the CMD is sufficient to assume that the volume estimation is reliable, and any error in the volume estimation would not exceed ±5% of our observed volume (Figure 2).

Contrary to the gypsum volume, our calculations show that the observed halite volume in the CMD can be deposited in a disconnected basin scenario. A CMD filled up to sill depth with water at halite saturation concentration (350 kg/m^3) would produce a volume of halite that is even bigger than observed (140%; Table 4). Three possible scenarios can reproduce our observations: (1) A CMD that undergoes evaporation and progressive drawdown with the consequent increase in salinity, reaching halite saturation concentration when the sea surface reaches the level of the sill (ca. 850 m; sill 01 in Figure 3) and the basin disconnects from the Mediterranean; (2) A full CMD at normal sea level having a stratified water column with depth-increasing salinities, where halite saturation is reached only at depths comparable with the depth of the deeper sill (sill 01 in Figure 3); (3) The volume of the halite deposit is not correlated to the volume of water at halite saturation and only appears to be by chance.

In the first scenario (1), our results show that blocking the outflow of ions from the CMD towards the Mediterranean (Figure 7) is enough to reach the halite saturation rapidly in the basin. Knowing that by the end of stage 1 the inflow salinity from the Mediterranean waters must have been very close to or even at gypsum saturation (see previous Section 5.1), the time to reach halite saturation can be as short as 1 kyr (Figure 7 and Table 5). This process of salinity increase must have been accompanied by a drawdown that reached at least the depth of the deep sill (ca. 850 m; sill 01 in Figure 3) and disconnected the CMD from the Mediterranean. Once the halite saturation is reached and the CMD is disconnected from the Mediterranean, the CMD starts precipitating the halite. The drawdown in the CMD now proceeds independently from the drawdown of the rest of the surrounding Mediterranean. Figure 6 shows that a quasi-desiccation in the CMD, and the subsequent halite deposition, would take place rapidly (ca. 1.2 kyr in the slowest case scenario) and that even the highest possible fresh water input by river would have a negligible effect on the amount of halite deposited.

In the second scenario (2), the basin is filled with water at halite saturation up to the sill depth and overlaid with a ca. 800 m thick column of relatively fresher water (<350 kg/m^3), sealing the brine off against atmospheric influence (i.e., evaporation). The brine, hence, is not affected by a sink of freshwater and needs a source of ions to surpass halite saturation and precipitate halite (see mechanism in Simon & Meijer, 2017). Such a source of ions

would need an area at the surface where water is so dense, that it is transported to the depth. This means that the stratification that characterizes this scenario would have to be broken at least locally and at least intermittently. Given the limited horizontal dimensions of the basin and the resulting salinity gradient in this case (due to its connection to the open Mediterranean), such a scenario is unlikely to take place in the CMD. This also applies to the double diffusion as a process (Arnon et al., 2016; Ouillon et al., 2019), for which the vertical salinity difference needs to be so small that the effect of temperature on density and saturation point cannot be ignored anymore (see mechanism in Arnon et al., 2016). In this case, in fact, the CMD would have to be inversely stratified with slightly higher salinity in the (warm) surface layer at least part of the year. Furthermore, the volume of the deposited halite would not depend on the water volume of the deep layer, but on the transports of ions into said volume. The more ions are imported to the volume, the more halite will be deposited. Such mechanisms observed in present-day evaporative basins (e.g., Dead Sea; Lensky et al., 2005; Sirota et al., 2018) are associated to high deposition rate of halite that can reach 0.15 m/yr (Table 2). Consequently, in such a scenario, the time needed to deposit the whole observed halite volume in the CMD is less than 2 kyr in the slowest case scenario, which is only 4% of the duration of stage 2 (ca. 50 kyr). Therefore, even if this mechanism is stopped (by drawdown and disconnection), an excess volume of halite would be produced, which is not observed in the present-day halite volume.

Scenario 3 (3) is similar, with the only difference being that the whole basin is assumed to be at halite saturation and long enough to precipitate the observed halite deposit. In this scenario, the inflow salinity has either to be very close to halite saturation or the fluxes from the Mediterranean to be small enough to increase the salinity locally in the CMD. Figure 10a shows that the magnitude of the fluxes from the CMD to the Mediterranean (Equation 7a) has to be $10^2\,m^3\,s^{-1}$ or smaller to reach halite saturation in the CMD when the Mediterranean inflow is still at gypsum saturation. With the cross sections of the connections between the CMD and the rest of the Mediterranean through the channels, this would require extremely slow horizontal velocities in the order of $v \approx 10^{-6}\,m^3/v$ and smaller (Figure 10b), which is the same order of magnitude as vertical velocities of the present-day global ocean (Liang et al., 2017). Horizontal velocities, however, tend to be much larger (e.g., River flows: $v_{river} \approx 10^0\,m/s$, Schulze et al., 2005; horizontal ocean currents: $v_{current} \approx 10^1\,m/s$, Lumpkin & Johnson, 2013; wind induced surface currents of the Dead Sea: $V_{DeadSea} \approx 10^{-2} - 10^{-1}\,m/s$, Padon & Ashkenazy, 2018). There is no reason to assume that the horizontal currents in the Western Mediterranean became slower than the sinking speed that is observed in the present-day global circulation. It is thus reasonable to assume that the inflow salinity in this scenario was at halite saturation. Again, given the short period of time needed to precipitate the halite deposit (Figure 10a), this high salinity inflow only needs to be reached for 150–1500 yrs to deposit the observed volume. The longer the connection lasts, the larger the deposited halite volume, which is something that we do not observe in the present-day halite volumes, hinting again that the CMD has to disconnect from the Mediterranean.

Our results supporting a quasi-desiccation of the CMD seem consistent with previously reported observations. Starting locally from the CMD itself, Raad et al. (2021) evidenced the presence of an erosional event truncating within the top of the halite unit in the depocentre of the CMD. The authors interpreted this erosion as due to subaerial exposure and/or dissolution of halite in relatively shallow water. Since our calculations show that no complete desiccation is possible due to river input (Figure 6), the subaqueous but shallow origin should be preferred. However, we cannot exclude that the salt was subaerially exposed on the flanks of the depocentre while a residual water body was present in its deeper part.

A similar observation from another intermediate-depth basin, the Caltanissetta Basin of Sicily, also supports an important sea level drawdown during the halite stage, where an erosional surface with desiccation cracks is cutting the top of a K- and Mg- salt rich level (Decima & Wezel, 1973; Garcia-Veigas et al., 1995; Lugli et al., 1999; Rouchy & Caruso, 2006). Some authors associated this erosional surface to the local desiccation of the Caltanissetta Basin (Manzi et al., 2012; Roveri et al., 2008) during stage 2. This is consistent with our interpretation and we propose that the Sicilian salt may have deposited during stage 2 in the Caltanissetta basin in a similar way to the one described above for the CMD (scenario 1), as both basins are classified as intermediate-depth and their MSC record share many similarities (Raad et al., 2021).

As long as the CMD is connected to the main Mediterranean basin, its water level will follow that of the Mediterranean. Studies showed evidences of a drawdown of even higher amplitudes than the depth of 850 m of our sill, varying from ca. 1500 m (Heida et al., 2021; Urgeles et al., 2011) up to quasi-desiccation of the deep basins (Pellen et al., 2019; Ryan, 1978). This means that the drawdown might have continued further in the Mediterranean, whereas the CMD had its own base level evolution as explained in Section 4.2 and shown in Figure 6. With the aim of evaluating the present-day observed halite volume in the frame of the consensus model (CIESM, 2008; Roveri, Flecker, et al., 2014), we performed a simple calculation, similar to the one done

for the CMD but on the scale of the whole Mediterranean, using the parameters presented in Table 6 and the mechanism in Figure 4b. We keep a restricted Mediterranean–Atlantic connection, allowing for an Atlantic inflow with a salinity of 35 kg/m^3 replacing the net freshwater loss (i.e., no drawdown; Meijer, 2012) for the whole MSC stage 2 duration (ca. 50 kyr as assumed in Roveri, Flecker, et al., 2014) where the Mediterranean waters are at halite saturation. Results of our calculations show that we would precipitate x1.5 times the observed deep basin evaporite volume ($977 \times 10^{+12}$ m^3, Table 6) calculated by Haq et al. (2020). This is not a contradiction to the results of Krijgsman and Meijer (2008), who used the same approach but estimated the volume of halite by combining the areal extent of halite as indicated by the distribution map of Rouchy and Caruso (2006), a thickness of 1000 m in the western basin and 3500 m in the eastern basin (after Lofi et al., 2005). Their calculated volume was close to the estimated one. Note that the volume given by Haq et al. (2020) includes the pre- and post-halite MSC units and it is thus an overestimation of the deep basin halite volume. Thus, we would expect to accumulate a volume of halite that could be at least two-times bigger than the observed one. However, the volume estimation by Haq et al. (2020) is more reliable and thus our calculation could be considered an improvement to Krijgsman and Meijer (2008). As for the CMD, our calculation suggests that the open Mediterranean could not have remained connected to the Atlantic during the whole duration of stage 2. Consequently, a drawdown must have occurred upon the Mediterranean's disconnection from the Atlantic because of the negative water budget that characterizes the Mediterranean (e.g., Krijgsman & Meijer, 2008; Meijer, 2006) and desiccation and refilling of the Mediterranean could have taken place very rapidly (within one precessional cycle; Meijer & Krijgsman, 2005). Of course, this calculation is very simplistic since it overlooks some factors such as the sill effect between the Eastern and Western Mediterranean (Blanc, 2000, 2006; Topper & Meijer, 2013), and the fact that the salt in the deep basin might have started deposition already during stage 1, at least in the eastern basin (Meilijson et al., 2019, 2022). Although, in their modelling of the MSC halite stage, Topper and Meijer (2013) tested the efficiency of the Siculo-Tunisian sill between the eastern and western Mediterranean basins and arrived to the same conclusion that a high amplitude drawdown (ca. 1500 m) must have happened at the end of halite deposition in the deep basin (see their Figure 10).

Another step to place the results obtained in the CMD in the wider context of the wider MSC events in the Western Mediterranean Basin is comparing the obtained halite volumes formed during water level drop in the CMD with those in the deep basin of the Western Mediterranean. The deep basin halite volume in the Western Mediterranean has been estimated at around 120×103 km^3 (Heida et al., 2021), which is considerably smaller than previous estimates (Haq et al., 2020). Using the reconstructed hypsometry of the western basin at the beginning of halite deposition derived from the paleo-bathymetry published in Heida et al. (2021), we can calculate the volume of halite that would result for different average starting salinities for the Western Mediterranean (Figure 11) for a disconnected basin that experiences drawdown (as in Figure 4a). For a low starting salinity model (190–210 kg/m^3) and halite saturation reached after a drawdown of ca. 850 m, a large drop in water level (>3000 m) is required to obtain >85% of the halite volume. A fully desiccated basin, which is physically impossible since the system would reach an equilibrium before (comparable to Figure 6), would also not lead to the total volume. This volume is only reached for a water column that starts precipitating after a drawdown of ca. 700 m or sooner which implies an average salinity of 232 kg/m^3 or higher (Figure 11). For a salinity of 350 kg/m^3, i.e., halite saturation, the drawdown needed to form the western Mediterranean MU halite is even reduced to 1600 m. This type of calculation simplifies a complex basin to one uniform water column and thus ignores effects like horizontal salinity differences, dynamic changes during the drawdown, like a continuous (even though reduced) supply of ions from the Atlantic to the deep Western Mediterranean Basin. This however, as well as our calculations on the CMD itself,

TABLE 6 Table showing the area and volume of the halite in the Mediterranean area

	Western mediterranean	Eastern mediterranean	References
Area covered by Halite (m^2)	5.38E + 11	2.80E + 11	Lofi (2018)
FWB (m^3/a)	−2.5[a] (10E + 15)E−3		Simon et al. (2017)
Volume of MSC evaporites (m^3)[a]	977E + 12		Haq et al. (2020)

Abbreviation: FWB, fresh water budget (calculated for both Western and Eastern Mediterranean).

[a]The volume of evaporites from Haq et al. (2020) includes pre-halite, halite and post-halite MSC units.

strongly indicate that halite did not start depositing before the beginning of the drawdown.

6 | CONCLUSIONS

We carried out numerical modelling of the Messinian Salinity Crisis (MSC) evaporites accumulation in the Central Mallorca Depression (CMD) using physics-based models built on conservation of mass of water and salt and a simplified model for the flow in sea straits. The interpretation of a widespread seismic dataset covering the CMD allowed the estimation of the volumes of the MSC evaporites that are used to constrain both our isostatic and evaporite precipitation models. According to the results and observations, we conclude the following:

- During stage 1 of the MSC (5.97–5.60 Ma), the upper water layer of the Mediterranean had to be at gypsum saturation salinity to supply the CMD with Ca^{2+} and SO_4^{2-} ions needed to deposit the observed volume of PLG. Gypsum deposition likely occurred only during part of precessional cycles (maximum duration of ca. 4.5 kyrs).
- The need of shallow topographic sills in the deposition of PLG appears not to be a pre-requirement, and PLG deposition was not necessarily limited to 200 m water depth but was rather constrained by the depth at which anoxia starts.
- Our results suggest that during stage 1, gypsum possibly deposited almost everywhere in the Mediterranean, including on open shelves. PLG may have successively been removed at any time by subaerial erosion or slopes instabilities, and re-sedimented in deeper contexts.
- The deep basin's Lower Unit traditionally associated to the MSC could thus at least partly be made of cumulatic and resedimented gypsum.
- Following the gypsum deposition, a phase of rapid base level drawdown commenced (beginning of stage 2; 5.60–5.55 Ma) accompanied with increasing salinities. The outflow of ions from the CMD towards the Mediterranean is blocked allowing halite saturation to be reached rapidly in the basin. After a period as short as ca. 1.5 kyr, the drawdown reached the depth of the basin sill lying at ca. 850 mbsl, leading to the complete disconnection of the CMD, and to halite precipitation.
- The base level in the CMD successively evolved separately from rest of the western Mediterranean Sea, still ongoing a drawdown. A quasi-desiccation in the CMD has likely been reached, and halite locally subaerially exposed while a residual water body was present in the deepest part.
- In the deep western Mediterranean basins, halite saturation was likely reached earlier than in the CMD in a basin strongly stratified before the beginning of the drawdown. Salt deposition, however, probably started after the beginning of the base-level drawdown, implying that salt deposition started in a relatively deep water context and ended when the acme of the drawdown was reached. Halite emplacement in the deep basin could have been completed before the end of stage 2.

On a larger basin scale, during stage 1 of the MSC, a normal, even though restricted, connection between the Atlantic and Mediterranean must have persisted, with no significant base level drop. This connection must have been further restricted until total interruption during stage 2, leading to the important base-level drop and the deposition of halite. Such drawdown must have led to the disconnection between the Western and Eastern Mediterranean basins during this stage, but halite deposition is not necessarily synchronous in both basins due to the further restriction imposed to the eastern basin by the Siculo-Tunisian sill as attested by several studies.

Even though many observations from the Balearic Promontory and the Western Mediterranean are coherent with the 3-step MSC consensus model, our results also highlight that some aspects of such model (e.g., limiting the PLG deposition to shallow >200 m silled basins; and the synchronous onset of the RLG and halite) may need to be reconsidered in future studies.

ACKNOWLEDGEMENTS

SALTGIANT ESRs and PIs are all thanked for the numerous exchanged discussions and comments during workshops, courses and fieldtrips. We are grateful to Andrew Madof and Francesco dela Pierre for their thorough and instructive review that improved a lot the quality of the manuscript. Fadl Raad and Ronja Ebner shared the primary responsibility for the modelling and writing of the manuscript. Paul Meijer oversaw and supervised the modelling procedure. Hanneke Heida, Johanna Lofi, Agens Maillard and Daniel Garcia-Castellanos helped in writing, reviewing and discussing the results of this work. All authors contributed to and made edits on the manuscript.

FUNDING INFORMATION

This research is carried out under the SALTGIANT ETN, a European project funded by the European Union's Horizon 2020 research and innovation programme under the Marie Skłodowska-Curie grant agreement number 765256. SaltGiant: www.saltgiant-etn.com

CONFLICT OF INTEREST

The authors certify that they have no affiliations with or involvement in any organization or entity with any financial or non-financial interest (such as personal or

professional relationships, affiliations, knowledge or beliefs) in the subject matter or materials discussed in this manuscript.

DATA AVAILABILITY STATEMENT

The data that support the findings of this study are available from the corresponding author upon reasonable request.

ORCID

Fadl Raad https://orcid.org/0000-0002-7143-2420
Ronja Ebner https://orcid.org/0000-0002-6361-761X
Hanneke Heida https://orcid.org/0000-0001-5456-896X

REFERENCES

Acosta, J., Canals, M., Carbó, A., Muñoz, A., Urgeles, R., Muñoz-Martín, A., & Uchupi, E. (2004). Sea floor morphology and Plio-Quaternary sedimentary cover of the Mallorca Channel, Balearic Islands, western Mediterranean. *Marine Geology*, *206*(1–4), 165–179. https://doi.org/10.1016/j.margeo.2004.02.008

Andreetto, F., Aloisi, G., Raad, F., Heida, H., Flecker, R., Agiadi, K., Lofi, J., Blondel, S., Bulian, F., & Camerlenghi, A. (2021). Freshening of the Mediterranean Salt Giant: Controversies and certainties around the terminal (Upper Gypsum and Lago-Mare) phases of the Messinian Salinity Crisis. *Earth-Science Reviews*, *216*, 103577.

Arnon, A., Selker, J. S., & Lensky, N. G. (2016). Thermohaline stratification and double diffusion diapycnal fluxes in the hypersaline Dead Sea. *Limnology and Oceanography*, *61*(4), 1214–1231. https://doi.org/10.1002/lno.10285

Artiaga, D., García-Veigas, J., Cendón, D. I., Atalar, C., & Gibert, L. (2021). The Messinian evaporites of the Mesaoria basin (North Cyprus): A discrepancy with the current chronostratigraphic understanding. *Palaeogeography, Palaeoclimatology, Palaeoecology*, *584*, 110681. https://doi.org/10.1016/j.palaeo.2021.110681

Bąbel, M., & Schreiber, B. C. (2014). Geochemistry of evaporites and evolution of seawater. In H. D. Holland, K. K. Turekian (Eds.), *Treatise on geochemistry* (Vol. *9*, 2nd ed., pp. 483–560). Elsevier. ISBN 9780080983004, https://doi.org/10.1016/B978-0-08-095975-7.00718-X

Bache, F., Olivet, J. L., Gorini, C., Rabineau, M., Baztan, J., Aslanian, D., & Suc, J.-P. (2009). Messinian erosional and salinity crises: View from the Provence Basin (Gulf of Lions, Western Mediterranean). *Earth and Planetary Science Letters*, *286*(1–2), 139–157. https://doi.org/10.1016/j.epsl.2009.06.021

Barceló-Llull, B., Pascual, A., Ruiz, S., Escudier, R., Torner, M., & Tintoré, J. (2019). Temporal and spatial hydrodynamic variability in the Mallorca Channel (Western Mediterranean Sea) from 8 years of underwater glider data. *Journal of Geophysical Research: Oceans*, *124*(4), 2769–2786. https://doi.org/10.1029/2018JC014636

Bellucci, M., Pellen, R., Leroux, E., Bache, F., Garcia, M., Do Couto, D., Raad, F., Blondel, S., Rabineau, M., Gorini, C., Moulin, M., Maillard, A., Lofi, J., Del Ben, A., Camerlenghi, A., Poort, J., & Aslanian, D. (2021). *A comprehensive and updated compilation of the seismic stratigraphy markers in the Western Mediterranean Sea* [Data set]. SEANOE. https://doi.org/10.17882/80128

Bigi, D., Lugli, S., Manzi, V., & Roveri, M. (2022). Are fluid inclusions in gypsum reliable paleoenvironmental indicators? An assessment of the evidence from the Messinian evaporites. *Geology*, *50*(4), 454–459. https://doi.org/10.1130/G49475.1

Bijma, J., Faber, W. W., & Hemleben, C. (1990). Temperature and salinity limits for growth and survival of some planktonic foraminifers in laboratory cultures. *Journal of Foraminiferal Research*, *20*(2), 95–116.

Blanc, P. L. (2000). Of sills and straits: A quantitative assessment of the Messinian Salinity Crisis. *Deep-Sea Research Part I: Oceanographic Research Papers*, *47*(8), 1429–1460. https://doi.org/10.1016/S0967-0637(99)00113-2

Blanc, P. L. (2006). Improved modelling of the Messinian Salinity Crisis and conceptual implications. *Palaeogeography, Palaeoclimatology, Palaeoecology*, *238*(1–4), 349–372. https://doi.org/10.1016/j.palaeo.2006.03.033

Blanc-Valleron, M.-M., Pierre, C., Caulet, J. P., Caruso, A., Rouchy, J.-M., Cespuglio, G., Sprovieri, R., Pestrea, S., & Di Stefano, E. (2002). Sedimentary, stable isotope and micropaleontological records of paleoceanographic change in the Messinian Tripoli Formation (Sicily, Italy). *Palaeogeography, Palaeoclimatology, Palaeoecology*, *185*(3), 255–286. https://doi.org/10.1016/S0031-0182(02)00302-4

Bulian, F., Sierro, F. J., Ledesma, S., Jiménez-Espejo, F. J., & Bassetti, M.-A. (2021). Messinian West Alboran Sea record in the proximity of Gibraltar: Early signs of Atlantic-Mediterranean gateway restriction. *Marine Geology*, *434*, 106430. https://doi.org/10.1016/j.margeo.2021.106430

Burollet, P. F., Said, A., & Trouve, P. (1978). Slim holes drilled on the Algerian shelf. In D. A. Ross & Y. P. Neprocnov (Eds.), *Initial reports of deep sea drilling project* (pp. 1181–1184). Government Press.

Calaforra, J. M., dell'Aglio, A., & Forti, P. (1993). Preliminary data on the chemical corrosion in gypsum karst: 1-The Sorbas region (Spain). In *XI International Congress of Speleology* (pp. 77–99). International Union of Speleology Chinese Academy of Sciences.

CIESM (2008). The Messinian salinity crisis from mega-deposits to microbiology. In F. Briand (Ed.), *A Consensus Report, in 33ème CIESM Workshop Monographs, 33., CIESM, 16, bd de Suisse, MC-98000, Monaco* (pp. 1–168).

Clauzon, G. (1978). The Messinian Var canyon (Provence, southern France)—Paleogeographic implications. *Marine Geology*, *27*(3), 231–246. https://doi.org/10.1016/0025-3227(78)90033-6

Clauzon, G., Suc, J. P., Couto, D. D., Jouannic, G., Melinte-Dobrinescu, M. C., Jolivet, L., Quillévéré, F., Lebret, N., Mocochain, L., Popescu, S. M., Martinell, J., Doménech, R., Rubino, J. L., Gumiaux, C., Warny, S., Bellas, S. M., Gorini, C., Bache, F., Rabineau, M., & Estrada, F. (2015). New insights on the Sorbas Basin (SE Spain): The onshore reference of the Messinian Salinity Crisis. *Marine and Petroleum Geology*, *66*, 71–100. https://doi.org/10.1016/j.marpetgeo.2015.02.016

Costanzo, A., Cipriani, M., Feely, M., Cianflone, G., & Dominici, R. (2019). Messinian twinned selenite from the Catanzaro Trough, Calabria, Southern Italy: Field, petrographic and fluid inclusion perspectives. *Carbonates and Evaporites*, *34*(3), 743–756. https://doi.org/10.1007/s13146-019-00516-0

De Lange, G. J., Boelrijk, N. A. I. M., Catalano, G., Corselli, C., Klinkhammer, G. P., Middelburg, J. J., Müller, D. W., Ullman, W. J., Van Gaans, P., & Woittiez, J. R. W. (1990). Sulphate-related

equilibria in the hypersaline brines of the Tyro and Bannock Basins, eastern Mediterranean. *Marine Chemistry*, *31*(1), 89–112. https://doi.org/10.1016/0304-4203(90)90032-8

De Lange, G. J., & Krijgsman, W. (2010). Messinian salinity crisis: A novel unifying shallow gypsum/deep dolomite formation mechanism. *Marine Geology*, *275*(1–4), 273–277.

Decima, A., & Wezel, F. C. (1973). Late Miocene evaporites of the Central Sicilian Basin, Italy. In A. G. Kaneps (Ed.), *Initial reports of the deep sea drilling project* (Vol. *13*, pp. 1234–1240). U. S. Government Printing Office. https://doi.org/10.2973/DSDP.PROC.13.144-1.1973

del Olmo, W. M. (2011). The Messinian in the Gulf of Valencia and Alboran Sea (Spain): Paleogeography and paleoceanography implications. *Revista de la Sociedad Geológica de España*, *24*, 22.

Dela Pierre, F., Bernardi, E., Cavagna, S., Clari, P., Gennari, R., Irace, A., Lozar, F., Lugli, S., Manzi, V., & Natalicchio, M. (2011). The record of the Messinian salinity crisis in the Tertiary Piedmont Basin (NW Italy): The Alba section revisited. *Palaeogeography, Palaeoclimatology, Palaeoecology*, *310*(3–4), 238–255.

Driussi, O., Briais, A., & Maillard, A. (2015). Evidence for transform motion along the South Balearic margin and implications for the kinematics of opening of the Algerian basin. *Bulletin de La Société Géologique de France*, *186*(4–5), 353–370. https://doi.org/10.2113/gssgfbull.186.4-5.353

Driussi, O., Maillard, A., Ochoa, D., Lofi, J., Chanier, F., Gaullier, V., Briais, A., Sage, F., Sierro, F., & Garcia, M. (2015). Messinian Salinity Crisis deposits widespread over the Balearic Promontory: Insights from new high-resolution seismic data. *Marine and Petroleum Geology*, *66, Part 1*, 41–54. https://doi.org/10.1016/j.marpetgeo.2014.09.008

Estrany, J., Garcia, C., Walling, D., & Ferrer, L. (2011). Fluxes and storage of fine-grained sediment and associated contaminants in the Na Borges River (Mallorca, Spain). *Catena*, *87*, 291–305. https://doi.org/10.1016/j.catena.2011.06.009

Frumkin, A. (1994). Hydrology and denudation rates of halite karst. *Journal of Hydrology*, *162*(1), 171–189. https://doi.org/10.1016/0022-1694(94)90010-8

Garcia, C., Amengual, A., Homar, V., & Zamora, A. (2017). Losing water in temporary streams on a Mediterranean Island: Effects of climate and land-cover changes. *Global and Planetary Change*, *148*, 139–152. https://doi.org/10.1016/j.gloplacha.2016.11.010

Garcia-Castellanos, D., Estrada, F., Jiménez-Munt, I., Gorini, C., Fernández, M., Vergés, J., & De Vicente, R. (2009). Catastrophic flood of the Mediterranean after the Messinian salinity crisis. *Nature*, *462*(7274), 778–781.

Garcia-Castellanos, D., & Villaseñor, A. (2011). Messinian salinity crisis regulated by competing tectonics and erosion at the Gibraltar arc. *Nature*, *480*(7377), 359–363. https://doi.org/10.1038/nature10651

Garcia-Veigas, F. J., Ortí, F., Rosell, L., Ayora, C., Rouchy, J. M., & Lugli, S. (1995). The Messinian salt of the Mediterranean: Geochemical study of the salt fromthe Central Sicily Basin and comparison with the Lorca Basin (Spain). *Bulletin de la Societe Geologique de France*, *166*, 699–710.

García-Veigas, J., Cendón, D. I., Gibert, L., Lowenstein, T. K., & Artiaga, D. (2018). Geochemical indicators in Western Mediterranean Messinian evaporites: Implications for the salinity crisis. *Marine Geology*, *403*, 197–214. https://doi.org/10.1016/j.margeo.2018.06.005

Gladstone, R., Flecker, R., Valdes, P., Lunt, D., & Markwick, P. (2007). The Mediterranean hydrologic budget from a Late Miocene global climate simulation. *Palaeogeography, Palaeoclimatology, Palaeoecology*, *251*(2), 254–267. https://doi.org/10.1016/j.palaeo.2007.03.050

Guibourdenche, L., Cartigny, P., Dela Pierre, F., Natalicchio, M., & Aloisi, G. (2022). Cryptic sulfur cycling during the formation of giant gypsum deposits. *Earth and Planetary Science Letters*, *593*, 117676. https://doi.org/10.1016/j.epsl.2022.117676

Haq, B., Gorini, C., Baur, J., Moneron, J., & Rubino, J.-L. (2020). Deep Mediterranean's Messinian evaporite giant: How much salt? *Global and Planetary Change*, *184*, 103052. https://doi.org/10.1016/j.gloplacha.2019.103052

Hardie, L. A., & Lowenstein, T. K. (2004). Did the Mediterranean Sea dry out during the Miocene? A reassessment of the evaporite evidence from DSDP legs 13 and 42A cores. *Journal of Sedimentary Research*, *74*(4), 453–461. https://doi.org/10.1306/112003740453

Heida, H., Raad, F., Garcia-Castellanos, D., Jiménez-Munt, I., Maillard, A., & Lofi, J. (2021). Flexural-isostatic reconstruction of the Western Mediterranean during the Messinian Salinity Crisis: Implications for water level and basin connectivity. *Basin Research*, *34*, 50–80. https://doi.org/10.1111/bre.12610

Hsü, K. J. (1973). The desiccated deep-basin model for the Messinian events. In C. W. Drooger (Ed.), *Messinian Events in the Mediterranean* (pp. 60–67). North Holland Publishing Co.

Knudsen, M. (1900). Ein hydrographischer lehrsatz. *Annalen der Hydrographie und Maritimen Meteorologie*, *28*(7), 316–320.

Krijgsman, W., Hilgen, F. J., Raffi, I., Sierro, F. J., & Wilson, D. S. (1999). Chronology, causes and progression of the Messinian salinity crisis. *Nature*, *400*(6745), 652–655.

Krijgsman, W., & Meijer, P. T. (2008). Depositional environments of the Mediterranean "Lower Evaporites" of the Messinian salinity crisis: Constraints from quantitative analyses. *Marine Geology*, *253*, 73–81. https://doi.org/10.1016/j.margeo.2008.04.010

La Violette, P. E. (1994). *Seasonal and interannual variability of the western Mediterranean Sea*. American Geophysical Union.

Lacombe, H., & Richez, C. (1982). The Regime of the Strait of Gibraltar. In J. C. J. Nihoul (Ed.), *Elsevier oceanography series* (Vol. *34*, pp. 13–73). Elsevier. https://doi.org/10.1016/S0422-9894(08)71237-6

Leeder, M. (1999). *Sedimentology and sedimentary basins: From turbulence to tectonics*. Blackwell Science. 592 pp.

Leeder, M. R. (2009). *Sedimentology and sedimentary basins: From turbulence to tectonics*. John Wiley & Sons.

Lensky, N. G., Dvorkin, Y., Lyakhovsky, V., Gertman, I., & Gavrieli, I. (2005). Water, salt, and energy balances of the Dead Sea. *Water Resources Research*, *41*(12), 1–13. https://doi.org/10.1029/2005WR004084

Liang, X., Spall, M., & Wunsch, C. (2017). Global ocean vertical velocity from a dynamically consistent ocean state estimate. *Journal of Geophysical Research: Oceans*, *122*(10), 8208–8224. https://doi.org/10.1002/2017JC012985

Lofi, J. (2018). *Seismic Atlas of the Messinian Salinity Crisis markers in the Mediterranean Sea—Volume 2: Vol. t.181 (C. for the G. M. of the World, Ed.)*. Société Géologique de France https://hal.archives-ouvertes.fr/hal-01975763

Lofi, J., Gorini, C., Berné, S., Clauzon, G., Tadeu Dos Reis, A., Ryan, W. B. F., & Steckler, M. S. (2005). Erosional processes and paleo-environmental changes in the Western Gulf of

Lions (SW France) during the Messinian Salinity Crisis. *Marine Geology*, *217*(1–2), 1–30. https://doi.org/10.1016/j.margeo.2005.02.014

Lofi, J., Sage, F., Déverchère, J., Loncke, L., Maillard, A., Gaullier, V., Thinon, I., Herve, G., & Guennoc, P. (2011). Refining our knowledge of the Messinian Salinity Crisis records in the offshore domain through Multi-site seismic analysis. *Bulletin de La Société Géologique de France*, *182*, 163–180. https://doi.org/10.2113/gssgfbull.182.2.163

Lüdmann, T., Wiggershaus, S., Betzler, C., & Hübscher, C. (2012). Southwest Mallorca Island: A cool-water carbonate margin dominated by drift deposition associated with giant mass wasting. *Marine Geology*, *307*, 73–87. https://doi.org/10.1016/j.margeo.2011.09.008

Lugli, S., Manzi, V., Roveri, M., & Schreiber, B. C. (2015). The deep record of the Messinian salinity crisis: Evidence of a non-desiccated Mediterranean Sea. *Palaeogeography, Palaeoclimatology, Palaeoecology*, *433*, 201–218. https://doi.org/10.1016/j.palaeo.2015.05.017

Lugli, S., Schreiber, B., & Triberti, B. (1999). Giant polygons in the Realmonte Mine (Agrigento, Sicily); evidence for the desiccation of a Messinian halite basin. *Journal of Sedimentary Research*, *69*, 764–771. https://doi.org/10.2110/jsr.69.764

Lugli, S., Vinicio, M., Marco, R., & Charlotte, S. B. (2010). The Primary Lower Gypsum in the Mediterranean: A new facies interpretation for the first stage of the Messinian salinity crisis. *Palaeogeography, Palaeoclimatology, Palaeoecology*, *297*(1), 83–99.

Lumpkin, R., & Johnson, G. C. (2013). Global ocean surface velocities from drifters: Mean, variance, El Niño–Southern Oscillation response, and seasonal cycle. *Journal of Geophysical Research: Oceans*, *118*(6), 2992–3006. https://doi.org/10.1002/jgrc.20210

Maillard, A., Driussi, O., Lofi, J., Briais, A., Chanier, F., Hübscher, C., & Gaullier, V. (2014). Record of the Messinian Salinity Crisis in the SW Mallorca area (Balearic Promontory, Spain). *Marine Geology*, *357*, 304–320. https://doi.org/10.1016/j.margeo.2014.10.001

Maillard, A., Gorini, C., Mauffret, A., Sage, F., Lofi, J., & Gaullier, V. (2006). Offshore evidence of polyphase erosion in the Valencia Basin (Northwestern Mediterranean): Scenario for the Messinian Salinity Crisis. *Sedimentary Geology*, *188–189*, 69–91. https://doi.org/10.1016/j.sedgeo.2006.02.006

Maillard, A., Raad, F., Chanier, F., Heida, H., Lofi, J., Mas, G., & Garcia-Castellanos, D. (2022). Plio-Quaternary strike-slip tectonics in the Central Mallorca Depression, Balearic Promontory: Land–sea correlation. *Tectonophysics*, *829*, 229295. https://doi.org/10.1016/j.tecto.2022.229295

Manzi, V., Gennari, R., Lugli, S., Persico, D., Reghizzi, M., Roveri, M., Schreiber, B. C., Calvo, R., Gavrieli, I., & Gvirtzman, Z. (2018). The onset of the Messinian salinity crisis in the deep Eastern Mediterranean basin. *Terra Nova*, *30*(3), 189–198.

Manzi, V., Gennari, R., Lugli, S., Persico, D., Roveri, M., Gavrieli, I., & Gvirtzman, Z. (2021). Synchronous onset of the Messinian salinity crisis and diachronous evaporite deposition: New evidences from the deep Eastern Mediterranean basin. *Palaeogeography, Palaeoclimatology, Palaeoecology*, *584*, 110685. https://doi.org/10.1016/j.palaeo.2021.110685

Manzi, V., Gennari, R., Lugli, S., Roveri, M., Scafetta, N., & Schreiber, B. C. (2012). High-frequency cyclicity in the Mediterranean Messinian evaporites: Evidence for solar–lunar climate forcing. *Journal of Sedimentary Research*, *82*(12), 991–1005. https://doi.org/10.2110/jsr.2012.81

Manzi, V., Lugli, S., Roveri, M., & Charlotte Schreiber, B. (2009). A new facies model for the Upper Gypsum of Sicily (Italy): Chronological and palaeoenvironmental constraints for the Messinian salinity crisis in the Mediterranean. *Sedimentology*, *56*(7), 1937–1960.

Manzi, V., Lugli, S., Roveri, M., Dela Pierre, F., Gennari, R., Lozar, F., Natalicchio, M., Schreiber, B. C., Taviani, M., & Turco, E. (2016). The Messinian salinity crisis in Cyprus: A further step towards a new stratigraphic framework for Eastern Mediterranean. *Basin Research*, *28*(2), 207–236. https://doi.org/10.1111/bre.12107

Manzi, V., Roveri, M., Argnani, A., Cowan, D., & Lugli, S. (2021). Large-scale mass-transport deposits recording the collapse of an evaporitic platform during the Messinian salinity crisis (Caltanissetta basin, Sicily). *Sedimentary Geology*, *424*, 106003. https://doi.org/10.1016/j.sedgeo.2021.106003

Marzocchi, A., Flecker, R., van Baak, C. G. C., Lunt, D. J., & Krijgsman, W. (2016). Mediterranean outflow pump: An alternative mechanism for the Lago-mare and the end of the Messinian Salinity Crisis. *Geology*, *44*(7), 523–526. https://doi.org/10.1130/G37646.1

Mas, G., & Fornós, J. J. (2020). The Messinian Salinity Crisis in Mallorca: New insights for a Western Mediterranean stratigraphic scenario. *Marine and Petroleum Geology*, *122*, 104656. https://doi.org/10.1016/j.marpetgeo.2020.104656

Mauffret, A. (1977). *Etude géodynamique de la marge des îles Baléares*. PhD thesis. Universite de Paris VI - Pierre et Marie Curie.

McCaffrey, M. A., Lazar, B., & Holland, H. D. (1987). The evaporation path of seawater and the coprecipitation of Br (super −) and K (super +) with halite. *Journal of Sedimentary Research*, *57*(5), 928–937. https://doi.org/10.1306/212F8CAB-2B24-11D7-8648000102C1865D

Meijer, P. (2006). A box model of the blocked-outflow scenario for the Messinian Salinity Crisis. *Earth and Planetary Science Letters*, *248*(1–2), 486–494. https://doi.org/10.1016/j.epsl.2006.06.013

Meijer, P. (2021). (Paleo)oceanography of semi-enclosed seas with a focus on the Mediterranean region; Insights from basic theory. *Earth-Science Reviews*, *221*, 103810. https://doi.org/10.1016/j.earscirev.2021.103810

Meijer, P., & Krijgsman, W. (2005). A quantitative analysis of the desiccation and re-filling of the Mediterranean during the Messinian Salinity Crisis. *Earth and Planetary Science Letters*, *240*(2), 510–520. https://doi.org/10.1016/j.epsl.2005.09.029

Meijer, P. T. (2012). Hydraulic theory of sea straits applied to the onset of the Messinian Salinity Crisis. *Marine Geology*, *326–328*, 131–139. https://doi.org/10.1016/j.margeo.2012.09.001

Meilijson, A., Liu, J., & Makovsky, Y. (2022). In and out of the salt: How to overcome stratigraphic uncertainty in evaporitic systems? A case study from the MSC in the deep levant basin. In *Conference of the Arabian Journal of Geosciences* (pp. 213–216). Springer. https://doi.org/10.1007/978-3-030-72547-1_47

Meilijson, A., Makovsky, Y., Steinberg, J., Bialik, O., Spaulding, S. A., Hilgen, F., Waldmann, N., Flecker, R., Boudinot, F. G., Fairbank, V., & Sepúlveda, J. (2019). Data for: Chronology with a pinch of salt: Integrated stratigraphy of Messinian evaporites in the deep Eastern Mediterranean reveals long lasting halite deposition during Atlantic connectivity, *1*. https://doi.org/10.17632/ngjtc2hzk9.1

Meilijson, A., Steinberg, J., Hilgen, F., Bialik, O. M., Waldmann, N. D., & Makovsky, Y. (2018). Deep-basin evidence resolves a 50-year-old debate and demonstrates synchronous onset of Messinian evaporite deposition in a non-desiccated Mediterranean. *Geology*, *46*(3), 243–246. https://doi.org/10.1130/G39868.1

Modestou, S., Simon, D., Gutjahr, M., Marzocchi, A., Kouwenhoven, T. J., Ellam, R. M., & Flecker, R. (2017). Precessional variability of $^{87}Sr/^{86}Sr$ in the late Miocene Sorbas Basin: An interdisciplinary study of drivers of interbasin exchange. *Paleoceanography*, *32*(6), 531–552. https://doi.org/10.1002/2016PA003061

Montadert, L., Letouzey, J., & Mauffret, A. (1978). Messinian event: Seismic evidence. *Initial Reports of the Deep Sea Drilling Project*, *42*, 1037–1050. https://doi.org/10.2973/dsdp.proc.42-1.154.1978

Mottershead, D. N., Duane, W., Inkpen, R. J., & Wright, J. S. (2005). Subaerial karstic erosion of small-scale saltrock terrains. In *6th International Conference on Geomorphology*, Zaragosa, Cardona, Spain, Abstract volume (p. 453).

Natalicchio, M., Dela Pierre, F., Lugli, S., Lowenstein, T. K., Feiner, S. J., Ferrando, S., Manzi, V., Roveri, M., & Clari, P. (2014). Did late miocene (Messinian) gypsum precipitate from evaporated marine brines? Insights from the piedmont basin (Italy). *Geology*, *42*(3), 179–182. https://doi.org/10.1130/G34986.1

Natalicchio, M., Pellegrino, L., Clari, P., Pastero, L., & Dela Pierre, F. (2021). Gypsum lithofacies and stratigraphic architecture of a Messinian marginal basin (Piedmont Basin, NW Italy). *Sedimentary Geology*, *425*, 106009. https://doi.org/10.1016/j.sedgeo.2021.106009

Ochoa, D., Sierro, F. J., Lofi, J., Maillard, A., Flores, J. A., & Suárez, M. (2015). Synchronous onset of the Messinian evaporite precipitation: First Mediterranean offshore evidence. *Earth and Planetary Science Letters*, *427*, 112–124. https://doi.org/10.1016/j.epsl.2015.06.059

Orti Cabo, F., Pueyo Mur, J. J., Geisler-Cussey, D., & Dulau, N. (1984). Evaporitic sedimentation in the coastal salinas of Santa Pola, Alicante, Spain. *Revista d'Investigacions Geologiques*, *38–39*, 9–29.

Ouillon, R., Lensky, N. G., Lyakhovsky, V., Arnon, A., & Meiburg, E. (2019). Halite precipitation from double-diffusive salt fingers in the Dead Sea: Numerical simulations. *Water Resources Research*, *55*(5), 4252–4265. https://doi.org/10.1029/2019WR024818

Padon, O., & Ashkenazy, Y. (2018). Non-hydrostatic effects in the Dead Sea. *Journal of Marine Systems*, *187*, 36–51. https://doi.org/10.1016/j.jmarsys.2018.06.007

Pellen, R., Aslanian, D., Rabineau, M., Suc, J. P., Gorini, C., Leroux, E., Blanpied, C., Silenziario, C., Popescu, S. M., & Rubino, J. L. (2019). The Messinian Ebro River incision. *Global and Planetary Change*, *181*, 102988. https://doi.org/10.1016/j.gloplacha.2019.102988

Pinot, J.-M., López-Jurado, J. L., & Riera, M. (2002). The CANALES experiment (1996-1998). Interannual, seasonal, and mesoscale variability of the circulation in the Balearic Channels. *Progress in Oceanography*, *55*(3), 335–370. https://doi.org/10.1016/S0079-6611(02)00139-8

Raad, F., Lofi, J., Maillard, A., Tzevahirtzian, A., & Caruso, A. (2021). The Messinian Salinity Crisis deposits in the Balearic Promontory: An undeformed analog of the MSC Sicilian basins?? *Marine and Petroleum Geology*, *124*, 104777.

Rouchy, J. M., & Caruso, A. (2006). The Messinian salinity crisis in the Mediterranean basin: A reassessment of the data and an integrated scenario. *Sedimentary Geology*, *188*, 35–67.

Roveri, M., Flecker, R., Krijgsman, W., Lofi, J., Lugli, S., Manzi, V., Sierro, F. J., Bertini, A., Camerlenghi, A., & De Lange, G. (2014). The Messinian Salinity Crisis: Past and future of a great challenge for marine sciences. *Marine Geology*, *352*, 25–58.

Roveri, M., Lugli, S., Manzi, V., & Schreiber, B. C. (2008). The Messinian Sicilian stratigraphy revisited: New insights for the Messinian salinity crisis. *Terra Nova*, *20*(6), 483–488.

Roveri, M., Manzi, V., Bergamasco, A., Falcieri, F. M., Gennari, R., Lugli, S., & Schreiber, B. C. (2014). Dense shelf water cascading and Messinian Canyons: A new scenario for the Mediterranean salinity crisis. *American Journal of Science*, *314*(3), 751–784. https://doi.org/10.2475/05.2014.03

Roveri, M., Manzi, V., Lugli, S., Schreiber, B., Caruso, A., Rouchy, J.-M., Iaccarino, S., Gennari, R., Vitale, F., & Lucchi, F. (2006). Clastic vs. Primary precipitated evaporites in the Messinian Sicilian basins. *L'Ateneo Parmense. Acta Naturalia: Organo Della Società Di Medicina e Scienze Naturali Di Parma*, *42*, 125–199.

Ryan, W. B. (1978). Messinian badlands on the southeastern margin of the Mediterranean Sea. *Marine Geology*, *27*(3), 349–363.

Ryan, W. B. F. (1973). Geodynamic implications of the Messinian crisis of salinity—Google Scholar. *Messinian Events in the Mediterranean*. https://scholar.google.com/scholar?hl=en&as_sdt=0%2C5&q=Geodynamic+implications+of+the+Messinian+crisis+of+salinity&btnG=

Ryan, W. B. F. (2009). Decoding the Mediterranean salinity crisis. *Sedimentology*, *56*(1), 95–136. https://doi.org/10.1111/j.1365-3091.2008.01031.x

Sàbat, F., Gelabert, B., Rodríguez-Perea, A., & Giménez, J. (2011). Geological structure and evolution of Majorca: Implications for the origin of the Western Mediterranean. *Tectonophysics*, *510*(1), 217–238. https://doi.org/10.1016/j.tecto.2011.07.005

Samperi, L., Giorgio, M., Kamaldeen, O. O., Alba, Z., Nicolas, W., Sabrina, N., Cristina, P., & Francesco, B. (2020). Estimation of the physical, petrophysical and mineralogical properties of Messinian salt rocks, Sicily: Implications for multidisciplinary applications. *Marine and Petroleum Geology*, *112*, 104032. https://doi.org/10.1016/j.marpetgeo.2019.104032

Sanna, L., De Waele, J., Calaforra, J. M., & Forti, P. (2015). Long-term erosion rate measurements in gypsum caves of Sorbas (SE Spain) by the Micro-Erosion Meter method. *Geomorphology*, *228*, 213–225. https://doi.org/10.1016/j.geomorph.2014.09.009

Schreiber, B. C., & Hsü, K. J. (1980). Evaporites. *Developments in Petroleum Geology*, *2*, 87–138.

Schulze, K., Hunger, M., & Döll, P. (2005). Simulating river flow velocity on global scale. *Advances in Geosciences*, *5*, 133–136.

Sierro, F., Flores, J. A., Francés, G., Vazquez, A., Utrilla, R., Zamarreño, I., Erlenkeuser, H., & Bárcena, M. Á. (2003). Orbitally-controlled oscillations in planktic communities and cyclic changes in western Mediterranean hydrography during the Messinian. *Palaeogeography, Palaeoclimatology, Palaeoecology*, *190*, 289–316. https://doi.org/10.1016/S0031-0182(02)00611-9

Sierro, F. J., Flores, J. A., Zamarreño, I., Vázquez, A., Utrilla, R., Francés, G., Hilgen, F. J., & Krijgsman, W. (1999). Messinian pre-evaporite sapropels and precession-induced oscillations in western Mediterranean climate. *Marine Geology*, *153*(1), 137–146. https://doi.org/10.1016/S0025-3227(98)00085-1

Simon, D., Marzocchi, A., Flecker, R., Lunt, D. J., Hilgen, F. J., & Meijer, P. T. (2017). Quantifying the Mediterranean freshwater budget throughout the late Miocene: New implications for sapropel formation and the Messinian Salinity Crisis. *Earth and Planetary Science Letters*, *472*, 25–37. https://doi.org/10.1016/j.epsl.2017.05.013

Simon, D., & Meijer, P. T. (2017). Salinity stratification of the Mediterranean Sea during the Messinian crisis: A first model analysis. *Earth and Planetary Science Letters*, *479*, 366–376. https://doi.org/10.1016/j.epsl.2017.09.045

Sirota, I., Enzel, Y., & Lensky, N. G. (2018). Halite focusing and amplification of salt layer thickness: From the Dead Sea to deep hypersaline basins. *Geology*, *46*(10), 851–854. https://doi.org/10.1130/G45339.1

Soria, J. M., Martín, J., Corbí, H., Dinarès-Turell, J., Lancis, C., Tent-Manclús, J., & Yébenes, A. (2008). The Bajo Segura Basin (SE Spain): Implications for the Messinian Salinity Crisis in the Mediterranean margins. *Stratigraphy*, *5*, 259–265.

Topper, R., Flecker, R., Meijer, P., & Wortel, M. (2011). A box model of the Late Miocene Mediterranean Sea: Implications from combined $^{87}Sr/^{86}Sr$ and salinity data. *Paleoceanography*, *26*, 1–16. https://doi.org/10.1029/2010PA002063

Topper, R., & Meijer, P. (2013). A modeling perspective on spatial and temporal variations in Messinian evaporite deposits. *Marine Geology*, *336*, 44–60. https://doi.org/10.1016/j.margeo.2012.11.009

Topper, R. P. M., & Meijer, P. T. (2015). The precessional phase lag of Messinian gypsum deposition in Mediterranean marginal basins. *Palaeogeography, Palaeoclimatology, Palaeoecology*, *417*, 6–16. https://doi.org/10.1016/j.palaeo.2014.10.025

Urgeles, R., Camerlenghi, A., Garcia-Castellanos, D., De Mol, B., Garces, M., Verges, J., Haslam, I., & Hardman, M. (2011). New constraints on the Messinian sealevel drawdown from 3D seismic data of the Ebro Margin, western Mediterranean. *Basin Research*, *23*(2), 123–145. https://doi.org/10.1111/j.1365-2117.2010.00477.x

Vargas-Yáñez, M., Juza, M., Balbín, R., Velez-Belchí, P., García-Martínez, M. C., Moya, F., & Hernández-Guerra, A. (2020). Climatological hydrographic properties and water mass transports in the Balearic Channels from repeated observations over 1996–2019. *Frontiers in Marine Science*, *7*, 1–22. https://www.frontiersin.org/article/10.3389/fmars.2020.568602

How to cite this article: Raad, F., Ebner, R., Heida, H., Meijer, P., Lofi, J., Maillard, A., & Garcia-Castellanos, D. (2023). A song of volumes, surfaces and fluxes: The case study of the Central Mallorca Depression (Balearic Promontory) during the Messinian Salinity Crisis. *Basin Research*, *35*, 1–27. https://doi.org/10.1111/bre.12702